AN ABSTRACT OF THE DISSERTATION OF

Valeriya Bychkova for the degree of Doctor of Philosophy in Chemistry
presented on November 21, 2011
Title: Polymeric Submicron Optical Ion-Selective Sensors.

Abstract approved:

James D. Ingle, Jr.

Ion-selective polymeric optical sensors – ion optodes – are a promising alternative to ion-selective electrodes and fluorescent dyes for analytical and biological applications, e.g. extra- and intracellular measurements. They are non-toxic, highly selective robust probes for ionic fluxes monitoring.

A large-scale fabrication of ion optodes using a solvent displacement method is introduced. This method is a single-batch process that does not require any additional steps. The influence of numerous parameters, e.g. surfactant concentration, solvent nature and membrane concentration, on the average size of the synthesized optodes was studied. The solvent displacement method allows control of the particle size in 200 nm to 30 μm range.

Ion optodes selective for sodium, potassium, and calcium cations were prepared and calibrated for hydrogen (pH), sodium, potassium, and calcium. Fabricated

sensors demonstrated excellent selectivity, low drift, high stability and reproducibility.

Further studies of ion-optodes of different sizes but the same chemical composition revealed a significant shift in their response function. This bias is clearly seen for all fabricated optodes. A strong correlation between a calculated specific surface area and the apparent ion-exchange constant was observed. Considering this, it may be hypothesized that the surface phenomena are contributing to the overall optode response resulting in the observed effect. As a consequence, the response models, developed for the macroscopic ion optodes, cannot be easily applied to the probes at micron- and nano-scale.

A primary concern for continuous sensing application of optical sensors is photobleaching of lipophilic fluorescent dye which prevents quantitative fluorescence measurements. Quantum dots, known for their high photostability, brightness and broad excitation spectra with narrow emission bands, were incorporated into polymeric matrix. They excited a fluorophore indirectly, thus, reducing its photobleaching and increasing sensors life-time. We created a composite, quantum dots doped, polymeric sensor that can be integrated into high-throughput detection platforms, such as flow cytometry, chip-based micro-total analysis system technologies, or bundled optical fiber arrays.

Ultimately, a fabricated ion-optode was introduced into a Boolean logic gate serving as a reporting microparticle. It responded to the pH changes generated *in situ* by the enzyme logic system. The present work aimed scaling down the size of biocomputing functional units which might reach the information processing by single molecules associated with signal-transducing single nanoparticles.

Polymeric Submicron Optical Ion-Selective Sensors

by

Valeriya Bychkova

A DISSERTATION

submitted to

Oregon State University

in partial fulfillment of

the requirements for the

degree of

Doctor of Philosophy

Presented November 21, 2011

Commencement June 2012

Doctor of Philosophy dissertation of Valeriya Bychkova

Presented on November 21, 2011

APPROVED:

Major Professor, representing Chemistry

Chair of the Department of Chemistry

Dean of the Graduate School

I understand that my dissertation will become part of the permanent collection of Oregon State University libraries. My signature below authorizes release of my dissertation to any reader upon request.

Valeriya Bychkova, Author

ACKOWLEDGEMENTS

I’m deeply indebted to my first research advisor, Dr. Alexey Shvarev, for his guidance and support. I appreciate his enthusiasm in my work and stimulating suggestions that helped to improve the quality of this work.

I gratefully thank Dr. James Ingle, Jr. for providing invaluable advice and helpful guidance in the progress of my research work.

A sincere acknowledgement is also extended to Dr. John Westall for his continuous help and discussions. The time and commitment of my graduate committee members: Dr. Vincent Remcho, Dr. John Westall, Dr. Paul Blakemore and Dr. Alex Yokochi, are greatly appreciated.

During my stay at OSU, I was fortunate to work with creative, intelligent and extremely supportive people. My special thanks go to all former Shvarev’s group members: Hasini Perera, Katy Fordyce and Natalia Pylypiuk for their friendship and advice. I extend my gratitude to the faculty and staff of Department of Chemistry, OSU.

I appreciate the Russian community in Corvallis, who provided a home-style environment in a foreign country and my many friends for their moral support throughout these years.

And most importantly, I would like to thank my family: my parents, Larysa and Viktor, – for their endless love, encouragement and confidence in me, and my brother Maksym – for always being an example and for being there for me, in all my ups and downs.

CONTRIBUTION OF AUTHORS

Dr. Alexey Shvarev assisted in writing and edited Chapters 2, 3, 5 of this dissertation. My research advisor, Dr. James D. Ingle, Jr., provided major assistance in interpreting data, editing and writing Chapter 4; Natalia Pylypiuk assisted with the data collection for pH and Na^+ response of quantum dots doped ion-optodes and studied pH susceptibility of quantum dots in suspensions. Jian Zhou, Marcos Pita and Dr. Evgeny Katz designed and tested the OR logic gate discussed in Chapter 5.

TABLE OF CONTENTS

TABLE OF CONTENTS (Continued)

Page

TABLE OF CONTENTS (Continued)

Page

TABLE OF CONTENTS (Continued)

Page

TABLE OF CONTENTS (Continued)

Page

LIST OF FIGURES

LIST OF FIGURES (Continued)

Figure Page

LIST OF TABLES

LIST OF APPENDIX FIGURES

Figure Page

CHAPTER 1

INTRODUCTION

1.1. Introduction

Living organisms have developed delicate and precise homeostatic systems to control the uptake, distribution, storage, and excretion of metal ions to maintain metal levels within physiological limits. Deviations in metal ion activities from normal homeostatic values in humans cause numerous diseases. Also, there is a growing interest in monitoring of signal transmitting ion fluxes the living cells. Consequently, a non-toxic highly selective and robust sensor that allows monitoring ion activities with negligible perturbation of the sample is needed. However, its development is extremely challenging.

Trends in analytical chemistry are moving towards extreme miniaturization of sensing devices. The domain of the sample is reduced to micrometer dimensions, e.g. cells and their compartments.

Significant progress in miniaturization of ion-selective electrodes (ISE's) and fiber-optic optodes has occurred recently.[1-4] While the tip of these sensors may have nanometer dimensions, mechanical and physical perturbation of the cell is caused by punching holes in cellular membrane during insertion. Additionally, the penetration volume of the sensor is a significant percentage of intracellular space. Maintaining cell viability, while monitoring more than one analyte in a single cell using nanocapillary ISE's or fiber optic nano-sensors, is even more significant challenge as several optodes must be inserted.

Injection of fluorescent indicator dyes into cells has provided insights into concentrations and special locations of ions within a single cell. These molecular probes have negligible volume relative to the cell volume but suffer from the chemical interference between the probe and cellular components. The dye itself may be toxic to the cell or specific cellular organelles. Also, many fluorescent probes are affected by self-quenching or by binding to protein while *in vivo*.[5]

PEBBLEs (photonic explorers for bioanalysis with biologically localized embedding) are a broad class of sensor particles that are designed for intracellular monitoring of small analytes[6] as an alternative to microelectrodes and fluorescent dyes. They have the potential of minimizing the physical and chemical interactions of small sensor probes or molecular probes, i.e. avoid physical and chemical interference with a sample. Ion-selective optical sensors (ion optodes) are a sub-class of PEBBLEs designed to monitor ions that lack good fluorescent indicators. Ion optodes are based on ISE's[7]— they utilize the same components and their response mechanisms rely on similar principles.[1] The ion optode matrix provides a protective coating for the sensing components preventing their interference with proteins. It also protects the cellular organelles, enabling the use of dyes that would usually be toxic. The ability to fabricate micron- and nano-sized spherical sensors results in minimal physical perturbation of the sample even when a large number of optodes is inserted into a single cell at one time. Nano-optodes offer a highly localized detection tool because they occupy just a fraction of a percent of the cell volume.[6] The composition of such sensors can be easily tuned, and multiple dyes and ionophores can be combined within the sensing phase to create complex sensing schemes.[8]

1.2. Sensing mechanism of ion optodes

The response of traditional ion optodes relies on concentration changes inside the bulk of a polymer phase (so-called bulk optodes). Such optodes are far superior to sensing approaches that use surface-attached indicators[9] because of the high selectivity that they impart with multiple sensing components. Furthermore, the equilibrium response time of the bulk optodes is limited in part by diffusion of the analyte within the liquid polymer membrane; therefore, a reduction in the

total membrane volume shortens the response also reducing a total cost of a sensor fabrication.

A large variety of anions, cations and neutral molecules can be determined by selective extraction into the polymer environment doped with an ionophore that is coupled to an optical readout mechanism. The higher sensitivity of fluorescence is well known, and its use in optical sensors provides means to significantly reduce the required membrane volume while retaining a good of signal-to-noise ratio (*S/N*).

Ionophore-based optical sensors typically contain one, two, or three active membrane components (Figure 1.1)[1]. One component systems (type I) are based on the incorporation of a lipophilic chromoionophore that has unique binding properties to one or more analytes and changes its optical properties as a result of the binding event. Examples for this system include electrically neutral H^+ chromoionophores, which may be used for anion or pH sensing purposes. They function according to an electrolyte co-extraction principle, where every uptake of a hydrogen ion must be accompanied by the co-extraction of a sample monovalent anion. Other one-component systems include ionophores with chromogenic groups that function as selective ion exchangers. Upon the uptake of an analyte ion, a hydrogen ion bound to a functionality of the ionophore is expelled, which alters the optical properties of the sensor.

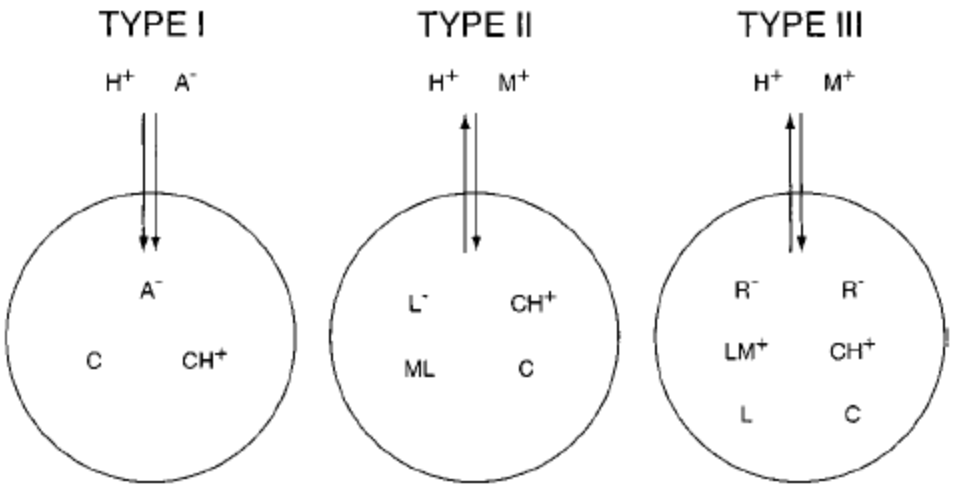

Figure 1.1. Schematic presentation of three different particle sensing mechanisms. The particle contains a neutral chromoionophore (C), charged or neutral cation-selective ionophore (L^- or L, respectively), and ion-exchanger (R^-). M^+ is a target metal ion.

Two-component sensing systems (type II) are often based on the incorporation of two selective ionophores, each selective for a particular ion, and one of them serving as the chromoionophore at the same time. For ion-exchange-based optodes, one of the two must be an electrically charged ionophore, while both ionophores are electrically neutral for electrolyte co-extraction optodes. Three-component optodes (type III) typically contain additional lipophilic ion exchangers (ionic sites), which provide the membrane with the necessary ion-exchange properties if the ionophores are all electrically neutral and, therefore, cannot function as ion exchangers. For sensors that function according to a co-extraction mechanism instead, ionic sites are required if one of the two ionophores is electrically charged. One obvious drawback of these sensors is their cross-sensitivity, which can be overcome by measuring pH simultaneously or by buffering the sample.

A wide range of neutral and electrically charged ionophores and pH-selective fluorophores is available that can be combined in sensing films to function according to a variety of sensing principles discussed above. The nature and concentration of the chromoionophore, the ionophore and the ion-exchanger control the optode response. Substituting a given chromoionophore by another one with different pK_a affects optode response. Thus, the dynamic working range can be tuned, and the detection limit can be improved. This approach leads to a highly versatile sensing approach.

1.3. Fabrication techniques

Production of ion optodes relies on advances in nano-scale production, using emulsion and dispersion fabrication techniques. However, the fabrication methods once optimized for a given matrix and its constituents are based on relatively simple wet chemistry techniques, as opposed to many complicated physical and chemical nanotechnology schemes. Several specific methods for producing sensors are described below.

In polyacrylamide (PAA) polymer sensors, a dye that has a chromometric response to an analyte is entrapped in the matrix pores.[6] The fabrication of PAA probes is based on emulsion techniques. Some control over particle size and shape can be gained by adjusting surfactant-to-water ratio in the emulsion.

Sol gel glasses have also been used as the matrix for the fabrication of ion optodes.[10] Their porosity, high purity, homogeneity and optical transparency make it an ideal choice for quantitative spectrophotometric measurements. Moreover, sol gel glass is chemically inert and more thermally stable than polymer matrices.

The use of fluorophores encapsulated in matrices mentioned above was proven valuable in the study of a number of intracellular analytes (H^+, Ca^{2+}, Zn^{2+}, O_2).[11-13] Unfortunately, fluorescent indicator dyes for many physiologically significant ions are not sufficiently selective or even unavailable.

Effective nano-sensors must often have complex compositions. However, in spite of their various advantages PAA and sol gel sensors, they cannot be used when multiple components with specific ratios need to be introduced in a sensor matrix.

This problem drives the development of decyl methacrylate (DMA) and poly(vinyl chloride) (PVC) liquid polymer sensors. Emulsion polymerization and solvent casting methods are widely used to produce plasticized and plasticizer-free DMA (using methyl methacrylate (MMA) as a DMA copolymer) sensing probes. Several cation-selective ionophores were evaluated in MMA-DMA matrix confirming that this plasticizer-free polymer matrix is suitable for ISE and ion optodes production.[14,15]

PVC has been the polymer most commonly used in membrane-based ISE's and ion optodes because of its high tensile strength, chemical inertness and compatibility with a wide range of plasticizers. Plasticized PVC is usually selected because it provides a lipophilic environment conductive for retention of active sensing components, and it has repeatedly been proven to be a suitable material for ionophore-based sensing.[1, 16] Traditionally, bis(2-ethylhexyl)sebacate (DOS) or *o*-nitrophenyloctylether (NPOE) are introduced into PVC matrix in a 1:2 ratio.[17] PVC-based spherical optodes were prepared under mild, nonreactive conditions using a particle casting process[18] which is based on a reproducible polymer drop formation and precipitation process. The method is a promising tool for mass-producing of polymer-based microspheres, however, the additional

equipment and time required to construct a particle casting apparatus complicates a fabrication process.

Herein, we focus on the development of plasticized polymer-based ion-selective sensors. A large-scale single-step method to fabricate polymeric ion optodes is introduced in Chapter 2. Its feasibility was tested with a PVC-DOS matrix. A possibility to control particle size in continuous manner in a wider range than reported previously[19] was discovered and explored.

1.4. Applications of optode nanoprobes

Potential biological applications for intracellular sensors in research and medicine are extensive. They include studying cellular dynamics, testing the effects of new drugs on single cells, monitoring embryos for birth defects, and gene sequence identification.[6]

An extensive variety of ion optodes selective to physiological electrolytes has been developed recently. They can reliably measure the most relevant cations (H^+, Na^+, K^+, Ca^{2+}, Mg^{2+})[2, 20-22], anions (Cl^-, I^-, NO_2^-)[23-25], and even neutral O_2 molecules.[26] These sensors can be used to measure electrolyte activity in bodily fluid (blood plasma, urine, saliva etc.), and could be extended to monitoring of dynamic ionic fluxes in between the cells. Nano-sized sensing particles allow measurements with minimal perturbation when the cells are in close proximity. Introduction of fabricated sensors into living cells to measure intracellular analytes was demonstrated.[13, 27] One of the most important considerations when applying optodes to single cell studies is the non-invasive delivery of the sensors to the cell. Many methods that have been explored include gene guns, pico-injection, liposomal delivery and sequestration into macrophages.[6] They vary in delivery complexity, cell viability and cost, but all are characterized by minor

mechanical and physical perturbation of the cell membrane and intracellular processes.

Ion optodes can also be used in environmental applications not involving single cells. The ongoing need for a fast and economical determination of heavy metals urges the development of optodes responsive to these elements. Environmental determination of heavy metals requires high selectivity, low detection limit, low cost and simplicity. Efforts were taken to develop ion optodes responsive to Ag^{+} ion.[28-30] Detection of Cu(II)[31], Hg(II)[28] and Pb(II)[32] utilizing optode sensing films was reported.

The potential utilization of nanometer-sized pH-sensitive sensors as transducers for the enzyme logic systems is discussed in Chapter 5. Miniaturization of biocomputing functional units while preserving their complexity and robustness will allow biomolecular computation at the level of a single molecule.

1.5. References.

(1) Bakker, E., Buhlmann, P., Pretsch, E. *Chem. Rev.* **1997**, *97*, 3083-3132.

(2) Shortreed, M., Bakker, E., Kopelman, R. *Anal. Chem.* **1996**, *68*, 2656-2662.

(3) Shortreed, M., Dourado, S., Kopelman, R. *Sensors Actuators B-Chemistry* **1997**, *38*, 8-12.

(4) Tan, W. H. S., Z.Y., Smith, S., Birnbaum, D., Kopelman, R. *Science* **1992**, *258*, 778-781.

(5) Ross, W. N. *Biophys. J.* **1993**, *64*, 1655-1656.

(6) Buck, S., Xu, H., Brasuel, M., Philbert, M.A., Kopelman, R. *Talanta* **2004**, *63*, 41-59.

(7) Morf, W. E., Seiler, K., Rusterholz, B., Simon, W. *Anal. Chem.* **1990**, *62*, 730-742.

(8) Ruedas-Rama, M. J., Wang, X., Hall, E, A.H. *Chem. Comm.* **2007**, 1544-1546.

(9) Goodey, A., Lavigne, J.J., Savoy, S.M., Rodriguez, M.D., Curey, T., Tsao, A., Simmons, G., Wright, J., Yoo, S., Sohn,Y., Anslyn, E.V., Shear, J.B., Neikirk, D. P., McDevitt, J.T. *J. Am. Chem. Soc.* **2001**, *123*.

(10) Xu, H., Aylott, J.W., Kopelman, R., Miller, T.J., Philbert, M.A. *Anal. Chem.* **2001**, *73*, 4124-4133.

(11) Clark, H. A., Barker, L.R., Kopelman, R., Hoyer, M., Philbert, M.A. *Sensors and Actuators B* **1998**, *51*, 12–16.

(12) Clark, H. A., Hoyer, M., Philbert, M.A., Kopelman, R. *Anal. Chem.* **1999**, *71*, 4831-4836.

(13) Clark, H. A. H., M., Parus, S., Philbert, M.A., Kopelman, R. *Mikrochimica Acta* **1999**, *131*, 121-128.

(14) Qin, Y., Peper, S., Bakker, E. *Electroanalysis* **2002**, *14*, 1375-1381.

(15) Peper, S., Ceresa, A., Qin, Y., Bakker, E. *Anal. Chim. Acta.* **2003**, *500*, 127-136.

(16) Seiler, K., Simon, W. *Anal. Chim. Acta.* **1992**, *266*, 73-87.

(17) Qin, Y., Bakker, E. *Talanta* **2002**, *58*, 909-918.

(18) Retter, R., Peper, S., Bell, M., Tsagkatakis, I., Bakker, E. *Anal. Chem.* **2002**, *74*, 5420-5425.

(19) Tsagkatakis, I., Peper, S., Retter, R., Bell, M., Bakker, E. *Anal. Chem.* **2001**, *73*, 6083-6087.

(20) Song, A., Parus, S., Kopelman, R. *Anal. Chem.* **1997**, *69*, 863-867.

(21) Dubach, J. M., Harjes, D.I., Clark, H.A. *Nano Lett.* **2007**, *7*, 1827-1831.

(22) Watts, A. S., Urbas, A.A., Moschou, E., Gavalas, V.G., Zoval, J.V., Madou, M., Bachas, L.G. *Anal. Chem.* **2007**, *79*, 8046-8054.

(23) Demuth, C., Spichiger, U.E. *Anal. Chim. Acta.* **1997**, *355*, 259-268.

(24) Wygladacz, K., Bakker, E. *The Analyst* **2006**, *132*, 268-272.

(25) Xu, C., Qin, Y., Bakker, E. *Talanta* **2004**, *63*, 180-184.

(26) Koo, Y. L., Cao, Y., Kopelman, R., Koo, S.M., Brasuel, M., Philbert, M.A. *Anal. Chem.* **2004**, *76*, 2498-2505.

(27) Brasuel, M., Kopelman, R., Miller, T.J., Tjakens, R., Philbert, M.A. *Anal. Chem.* **2001**, *73*, 2221-2228.

(28) Lerchi, M., Reitter, E., Simon, W., Pretsch, E., Chowdhurry, D.A., Kamata, S. *Anal. Chem.* **1994**, *66*, 1713-1717.

(29) Shamsipur, M., Rouhani, S., Mohajeri, A., Ganjali, M.R. *Anal. Bioanal. Chem.* **2003**, *375*, 692-697.

(30) Wygladacz, K., Radu, A., Xu, C., Qin, Y., Bakker, E. *Anal. Chem.* **2005**, *77*, 4706-4712.

(31) Méallet-Renault, R., Hérault, A., Vachon, J., Pansu, R.B., Amigoni-Gerbier, S., Larpent, C. *Photochem. Photobiol. Sci.* **2006**, *5*, 300-310.

(32) Anticó, E., Lerchi,M., Rusterholz, B., Achermann, N., Badertscher, M., Valiente, M., Pretsch, E. *Anal. Chim. Acta.* **1999**, *388*, 327-338.

CHAPTER 2

FABRICATION OF MICROMETER AND SUBMICROMETER-SIZED ION-SELECTIVE OPTODES VIA A SOLVENT DISPLACEMENT PROCESS

Valeriya Bychkova, Alexey Shvarev*

Analytical Chemistry

American Chemical Society

1155 16th Street N.W., Washington, DC 20036

Volume 81(**2009**), Issue 6, 2325–2331

2.1. Abstract

Microsphere-based ion optodes represent a promising and versatile tool to measure ionic activities in confined samples. The reported methods of micro- and nanosphere optode fabrication, however, suffer from various degrees of complexity. We propose a large-scale fabrication of polymeric ion-selective optodes using a solvent displacement method. Plasticized poly(vinyl chloride) along with the optode components was dissolved in a solvent miscible with water. Injection of a polymer solution into a stirred aqueous phase containing a surfactant causes spontaneous emulsification. This technique does not require additional preparation steps and allows one to control the composition of the sensor matrix precisely. Several factors affecting the particle size distribution are examined such as composition of continuous and disperse phases. The concentration of the polymer in the organic solvent and the choice of the solvent nature allowed us to control the particle size distribution within 200 nm-30 μm. The concentration and the nature of the surfactant had a little influence on the particle size distribution. We fabricated three different batches of ion-selective optodes using chromoionophore I, lipophilic ion-exchanger and sodium ionophore X, BME-44, and ETH 5234 for sodium, potassium, and calcium optodes, respectively. The sensors were fully functional with excellent selectivity to interfering ions.

2.2. Introduction

Ion-selective optical sensors (ion optodes) are based on the same compounds (ion carriers, ion-exchangers, etc.)[1] and response mechanisms[2] as ion-selective electrodes. For example, a regular cation-selective optode[2] contains an ionophore, which selectively binds a primary ion and a second ionophore (chromoionophore) that interacts with a reference ion (usually, hydrogen) and

changes optical properties. The competition between the two ions for ion-exchange sites in the optode matrix determines the sensor response.

A wide range of ion optodes have been developed1 over the past [2] decades for the detection of cations, anions, and even neutral analytes. Typically, these sensors have been fabricated as thin polymeric films on transparent substrates,[3] as miniature probes at the tip of an optical fiber.[4]

Trends in modern analytical chemistry are moving toward extreme miniaturization of sensing devices. Microsphere-based analytical assays represent an important, versatile, and powerful research tool.[5,6] They require extremely small amounts of samples and offer localized recognition chemistry both spatially and temporally. The signal acquisition can be performed in a massively parallel fashion using optical imaging recognition and processing techniques.[7] Sensing microparticles can be manipulated with fluidics, with a conventional flow cytometry[8] or laboratory-on-chip devices.[9]

Miniaturization of ion-selective optodes in a form of micrometer and submicrometer-sized polymeric beads was proven a success. [10-14] Recently, it was demonstrated that thousands of such beads can be injected into a living cell without significant perturbation, thus allowing one to monitor intracellular activities of ionic species.[10,11]

Several different techniques were employed in order to fabricate polymeric sensing particles including dispersion[15,16] and emulsion polymerization.[10,11,17] Emulsion polymerization yields smaller particles from 20 to 100 nm in diameter, while dispersion polymerization generates larger microspheres ranging from 100 nm to 100 μm. Although emulsion or dispersion polymerization is a relatively simple process, an additional step (swelling) is necessary in order to introduce the sensing components (ionophore, ion-exchanger, chromoionophore) into the polymeric matrix. Introducing the components in a single-batch process

greatly increase the risk of decomposition due to harsh reaction conditions such as high temperature and UV-radiation.

An alternative technique or so-called particle casting was used by Bakker and co-workers.[12,16] This method utilizes the instability of a liquid jet formed by a solution of a polymer in organic solvent (dichloromethane). The jet is formed when the solution is forced to flow into an aqueous phase through the ceramic capillary 1-50 μm in diameter under external pressure of 3-4 bar. The liquid jet is periodically disturbed by means of an oscillating piezoelectric transducer at a frequency of 10-100 kHz. The jet forms highly monodisperse polymer droplets at a rate of 20,000 droplets/s. However the minimum particle size in the latter method is limited to a capillary diameter, which imposes a practical limit to the production of submicrometer-sized particles.

We propose a simple method for the fabrication of ion-selective optodes, which does not suffer the abovementioned disadvantages. The solvent displacement method,[18-20] is a simple single-batch process. The ion-selective sensors can be fabricated with a relatively good yield without additional procedures such as swelling. Surprisingly, this well-known method was not used in the area of ion-selective chemical sensors. We decided to explore this method after numerous observations of spontaneous emulsification when a solution of poly(vinyl chloride) in THF was accidentally mixed with water.

2.3. Experimental section

2.3.1. Reagents.

High-molecular weight poly(vinyl chloride)(PVC), bis(2-ethylhexyl) sebacate (DOS), *tert*-butyl calix[4]arene tetraethyl ester (sodium ionophore X), 2-dodecyl-2-methyl-1,3-propanediyl bis[*N*-[5′-nitro(benzo-15-crown-5)-4′-yl]carbamate]

(BME-44, potassium ionophore), calcium ionophore *N*,*N*-dicyclohexyl-*N*′,*N*′-dioctadecyl-3-oxapentanediamide (ETH 5234), sodium tetrakis-[3,5-bis(trifluoromethyl)phenyl borate (NaTFPB), 9-(diethylamino)-5-octadecanoylimino-5*H*-benzo[*a*]phenoxazine (chromoionophore I, ETH 5294), tetrahydrofuran (THF), cyclohexanone, ethylene glycol diethyl ether, acetone, Brij-35, sodium dodecylsulfate, Triton-X, and polyethylene glycol 5000 monomethyl ether (PEG 5000) were from Aldrich (Milwaukee, WI). All other chemicals were purchased from VWR (West Chester, PA). Aqueous solutions were prepared by dissolving the appropriate salts in deionized water (18.2 MΩ cm).

2.3.2. Preparation of membrane cocktail.

The sensor components, polymer (PVC), and the plasticizer were dissolved in 1 mL of a 2:1 mixture of cyclohexanone and ethylene glycol diethyl ether. Specifically, the sodium-selective cocktail contained 40 mmol/kg of sodium ionophore X, 20 mmol/kg of ion-exchanger NaTFPB, and 10 mmol/kg of chromoionophore I. The potassium-selective cocktail contained of 30 mmol/kg of BME-44, 15 mmol/kg of NaTFPB, and 7.5 mmol/kg of chromoionophore I. The composition of calcium-selective cocktail consisted of 22 mmol/kg of calcium ionophore ETH 5234, 7 mmol/kg of ion-exchanger NaTFPB, and 4.5 mmol/kg of chromoionophore I.

2.3.3. Fabrication of the optode beads.

Different organic solvents including THF, acetone, cyclohexanone, or ethylene glycol diethyl ether were added to dilute the membrane cocktail in the range from 1:1 to 1:10. A small (~8 mL) vial was filled with a solution of a surfactant in

deionized water. The aqueous solution was stirred using a small magnetic stir bar at approximately 100 rpm. A small amount of the polymer solution was drawn into a disposable syringe with the attached needle. The syringe was held above the vial, the needle was not immersed into the aqueous phase being positioned at 4-5 mm above the solution surface, and the polymeric solution was rapidly injected. Within seconds precipitation and formation of a milky emulsion was observed along with a small amount of coagulum. The emulsion was filtered using a Whatman no. 1 filter and used.

We studied the possibility to obtain a tighter distribution of the particles using different filters. The initial emulsion was further vacuum-filtered using a Whatman no. 3 cellulose filter (pore size 6 μm) and Whatman no. NL17 polyamide membrane (pore size 0.45 μm).

2.3.4. Particle size distribution.

We performed the size characterization using the low-angle laser light scattering (LALLS) method in order to characterize the size distribution within the 50 nm-50 μm range. All of the measurements were carried out using the Hydro 2000S-AWA 2001 particle size analyzer and Mastersizing 2000 software (Malvern Inst., Westborough, MS).

2.3.5. Instrumentation.

The custom-made flow cell (similar to VacuCel produced by C&L Instruments, Hershey, PA) was used to hold a microscope cover glass. The cell was connected to a peristaltic pump (Variable-Flow MiniPump, Fisher Scientific, Pittsburgh, PA) operating at 0.1 mL/s. The measurements were carried out in a “stop-flow”

mode. The pH was measured using a pH-meter (Accumet XL-15, Fisher Scientific, Pittsburgh, PA) with a double-junction combination glass pH-electrode.

The optical setup included an inverted fluorescence microscope (Olympus IX-71, Olympus, Center Valley, PA) with attached microspectrometer (Acton Microspec MS-2150) and PIXIS-512 cooled CCD camera (both from Princeton Instruments, Trenton, NJ). The microspectrometer allows simple switching between direct imaging (non-dispersed) and spectral imaging (dispersed) modes. A mirror and a diffraction grating are attached to the motorized computer-controlled turret providing fast switching capability; thus, the same camera can be used for both direct and spectral imaging.

A fast wavelength switch DG-4 (Sutter Instrument, Novato, CA) with a 300 W xenon arc lamp and 535 (±25) nm filter was used a light source. A filter cube consisted of a 565 nm dichroic mirror and 600 nm long-pass emission filter. The microscope was equipped with 40×/0.17 objective (UPlanSApo, Olympus, Center Valley, PA).

The camera and the spectrometer were controlled by a PC running WinSpec32 software (Princeton Instruments, Trenton, NJ) in the slave mode. A custom-programmed microcontroller was used to control DG-4 and generate triggering signals for the CCD camera. The detection was performed with a 220 ms pulse of excitation light (550 nm) with simultaneous triggering of the camera shutter for 200 ms exposure.

At first, the microspectrometer was switched in the direct imaging mode. To avoid photobleaching, the continuously acquired image was examined in the transmission mode and a particle of interest was selected. Then the microscope stage was moved in order to position the particle in the center, and the slit was

placed at the spectrometer entrance. The setup was switched to the fluorescence mode, and the fluorescence spectrum was acquired.

Working with the mechanical microscope stage, we found the accurate particle positioning to be one of the most challenging experimental problems. In order to achieve better control and accuracy, we needed to replace the original mechanical stage. We used a home-built combination of the motorized stage (H107, Prior Scientific, Rockland, MA) and piezoelectric stage (P517-K024, Physik Instrumente, Irvine, CA). The mechanical positioned allowed a coarse displacement within ±20 mm with ±1 μm resolution. The piezoelectric stage had a 100 μm throw with a 1 nm closed-loop resolution. In practice, the latter was limited to ±25 nm due to the resolution of the 12-bit DAC (USB-6009, National Instruments, Austin, TX) used to control the analog piezoelectric stage controller.

The long-pass filter in the fluorescence cube allowed us to record the spectra within the 600-800 nm region. The fluorescence of the chromoionophore was measured at 650 and 680 nm that corresponds to the fluorescence maxima[16] of the deprotonated and protonated forms of the dye.

2.3.6. Optode response measurements.

A typical cation-selective optode[2] contains an ionophore *L*, which selectively forms a complex with a primary (metal) ion I^{z+}, and a chromoionophore *Ind*, a lipophilic dye that interacts with a reference ion (usually, hydrogen) and undergoes changes in optical properties upon protonation. The third additive is a lipophilic cation-exchanger. Since the concentration of ion-exchanger in the matrix is limited, the competition between two ions for the ion-exchange sites affects the fraction of protonated chromoionophore $IndH^+$ and determines the sensor response. If the pH in the aqueous sample is fixed (buffered), the optode

responds to the metal activity in the sample or vice versa. With the assumption that n_I is the stoichiometry of the ion-ionophore complex and z_I is the charge of the primary ion, the theoretical optode response function obeys the following equation:[14]

$$a_I = (z_I K_{exch})^{-1} \left(\frac{\alpha}{1-\alpha} a_H\right)^{z_I} \left(\frac{R_T - (1-\alpha) Ind_T}{\left\{ L_T - (R_T - (1-\alpha) Ind_T) \left(\frac{n_I}{z_I}\right) \right\}^{n_I}} \right) \quad (2.1)$$

where K_{exch} is the ion-exchange constant. The subscript T denotes the total concentrations of the ionophore (*L*), the ion-exchanger (*R*), or the chromoionophore (*Ind*). The symbols a_I and a_H represent the activities of the cation I^{z+} and hydrogen in the aqueous phase, respectively. The mole fraction of the protonated form of the chromoionophore is related to the fluorescence signal as

$$1 - \alpha = \frac{[IndH^+]}{Ind_T} = 1 - \frac{F_{max} - F}{F_{max} - F_{min}} \quad (2.2)$$

where F is a fluorescence intensity ratio (at two wavelengths) measured in a given experiment, F_{min}, and F_{max} are the fluorescence intensity ratios at the minimum and maximum protonation of the chromoionophore, respectively, [IndH+] is the concentration of the protonated form of the chromoionophore. The intensity ratios at the minimum and maximum protonation were measured in 0.01 M solutions of NaOH and HCl, respectively.

The pH of the solutions was maintained with 10 mM of TRIS and MOPS buffers. All experiments were conducted at ambient temperature (23 ± 2 °C). Activity coefficients were calculated according to Debye-Hückel formalism.[21]

2.4. Results and discussion

The solvent displacement method[19,20] involves two essential steps (Figure 2.1). During the first step, a preformed hydrophobic polymer is dissolved in a solvent miscible with water. Injection of a polymer solution into a stirred aqueous phase causes spontaneous emulsification. Polymer deposition at the interface between the organic (disperse) and aqueous (continuous) phases instantaneously produces a colloidal suspension. A surfactant is usually added to the aqueous phase in order to stabilize the emulsion. The solvent diffuses into the aqueous phase causing the micro or nanospheres to precipitate.

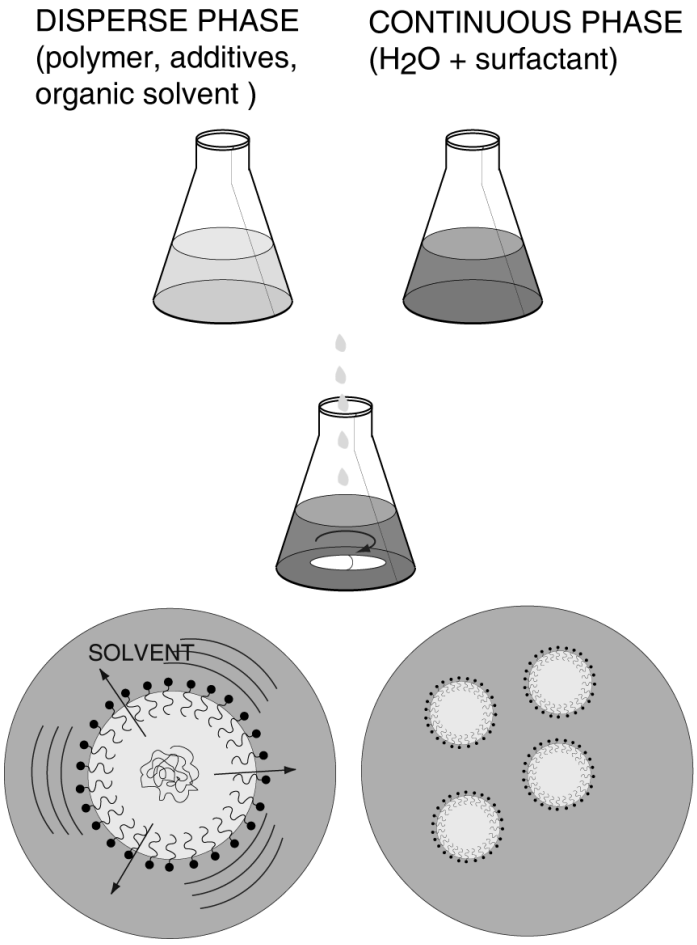

Figure 2.1. Fabrication of polymeric particles via a solvent displacement method.

One of the main requirements for a polymer choice is a substantial difference in hydrophobicity between a disperse phase and continuous phase. In other words, a polymer must be very hydrophobic to be dispersed in aqueous solution. The second requirement is a continuous miscibility of a polymer solvent with water. In this sense, hydrophobic polymers, which are used for the optode matrix such as PVC or polyacrylates along with typical solvents such as THF or cyclohexanone, represent an ideal choice for the emulsion fabrication via solvent displacement.

The main advantage of this technique is that all of the sensor components (ionophore, ion-exchanger, pH-sensitive dye) can be dissolved in the disperse phase simultaneously producing ready-to-use sensor particles. It is hard to imagine a method that will be simpler than a direct injection of polymeric solution into an aqueous phase forming a stable emulsion of the sensor particles in a few seconds.

Here we report on a successful application of this method to the fabrication of micrometer and submicrometer-sized ion-selective optodes. Plasticized PVC was chosen because it is a widely used as a matrix for the polymeric membranes of the ion selective electrodes and ion optodes. However, alternative hydrophobic membrane materials such as polysiloxanes and polyacrylates can be possibly processed via solvent displacement as well. A ratio of plasticizer/PVC of 2:1 was used due to the combination of excellent transport properties and good mechanical stability. We explored how the size distribution of the polymeric particles is affected by the composition of both disperse (polymeric) and continuous (aqueous) solutions.

In a series of preliminary experiments, PVC and the plasticizer were dissolved in an appropriate organic solvent and injected into an aqueous phase containing a surfactant. Polymer precipitation following the solvent displacement

instantaneously produced an emulsion containing spherical particles of various size. A typical batch of particles fabricated from the dissolving of membrane cocktail in cyclohexanone is shown in Figure 2.2 in both bright field and fluorescence modes. Clearly, the majority of the particles are spherical ranging from 1 to 10 μm. In order to take the picture, a droplet of the emulsion was deposited on a coverslip and the sample was partially dried to increase the density of the emulsion. Under this condition, small particles (<1 μm) formed aggregates on the glass surface. However, we did not observe any aggregation in the solution.

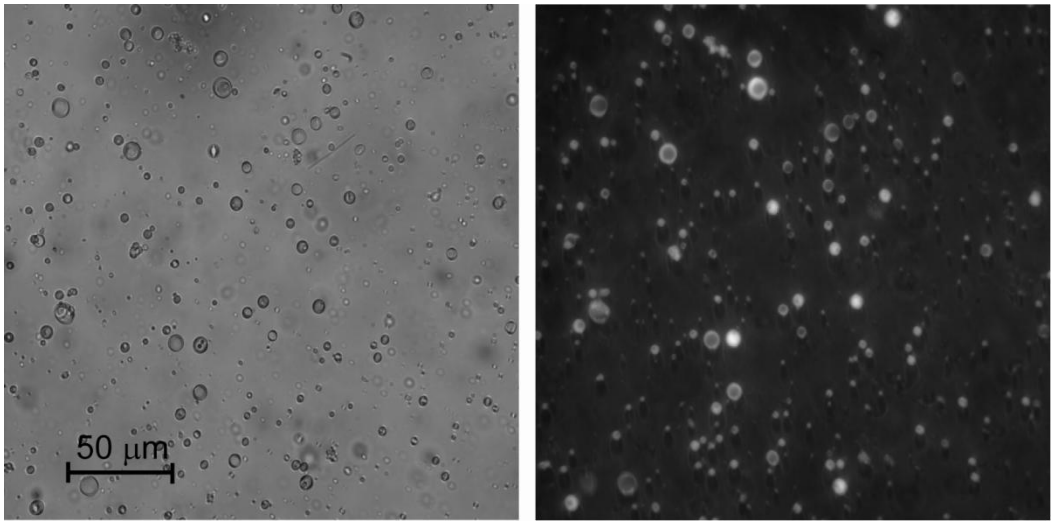

Figure 2.2. A bright field (left) and fluorescence (right) images of the polymeric particles prepared via solvent displacement from the cocktail diluted with 1:1 THF. The continuous phase contains 0.01% of Brij-35 (40x objective, the particles are doped with Chromoionophore I, excitation at 550 nm, the image is captured using 600 nm emission filter). The ambient red light caused the shadows to appear on the fluorescence image.

At relatively high concentrations of the polymeric solution, a formation of coagulum followed the spontaneous emulsification. The dilution of the optode cocktail substantially reduced the amount of coagulum increasing the

emulsification yield up to 80%. In the absence of a surfactant, larger amounts of coagulum were observed. Moreover we observed aggregation and precipitation of the particles over time. After addition of a surfactant at relatively low concentration within 0.001-0.01% wt, the emulsification yield substantially increased and stability of the emulsion was improved. Regardless of the particle size distributions, the emulsions lifetime exceeded 1 week. Further increase in the surfactant concentration apparently did not cause any improvements in terms of yield and stability. This is probably an important advantage of this method because higher concentrations of surfactants may interfere with the ionophores and affect the selectivity.[22] Indeed, at concentrations higher than 0.1% we observed the interference of the neutral surfactants such as Triton X and Brij-35 with the sodium-selective ionophore.

After systematic studies of the size distribution of the PVC particles, we concluded that despite the simplicity of the method and lack of control of the mixing rate, the resulting size distribution was quite reproducible for a given composition of both phases. The reproducibility was tested by repeated injections of the polymeric solution and analyzing the resulting size distribution in the emulsion. For example, the membrane cocktail diluted with 1:1 THF produced the particles in which the size distribution is shown in Figure 2.3 for two consecutive trials. The size distribution was in most cases unimodal with moderate degree of monodispersity. Dilution with cyclohexanone or ethylene glycol diethyl ether yielded a similar reproducibility and distribution pattern.

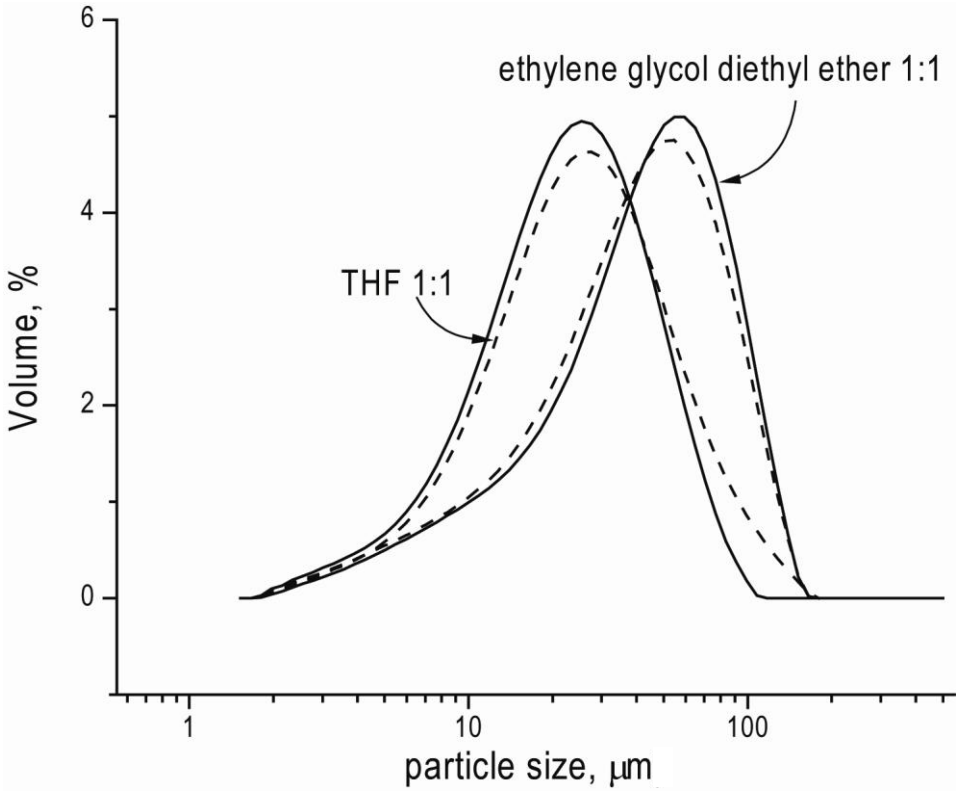

Figure 2.3. The reproducibility of the particle size distribution for two batches and two different compositions of the dispersed phase.

Apparently, the nature of the solvent apparently has the strongest influence on the size of the particles. Figure 2.4 illustrates the size distribution obtained when the membrane cocktail was diluted 1:10 with cyclohexanone, ethylene glycol diethyl ether, THF, and acetone. Acetone and THF allowed the production of particles in the submicrometer range with an average diameter of 180 nm. These emulsions appeared milky due to the Rayleigh scattering. One of the possible explanations is that the particle size is controlled by the mutual diffusion of organic solvent and water and therefore by a local mixing rate.

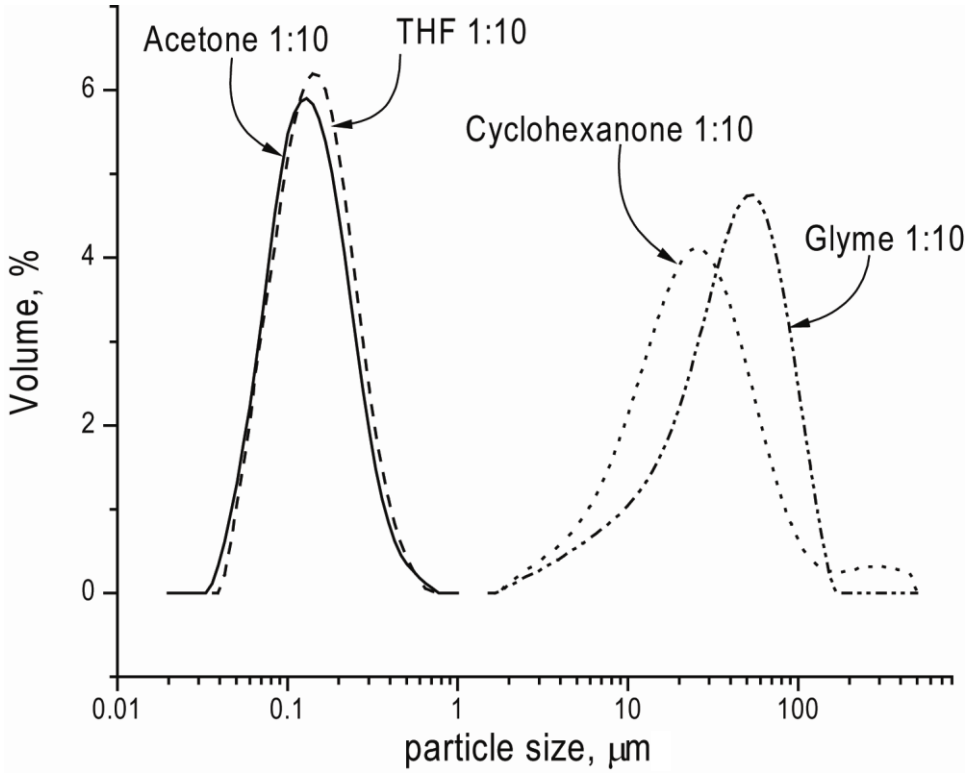

Figure 2.4. The effect of the solvent nature on the particle size distribution for acetone, THF, cyclohexanone, and ethylene glycol diethyl ether. In each case the cocktail was diluted 1:10 with the organic solvent. The submicron-sized particles were further purified using Whatman # NL17 polyamide membrane (pore size 0.45 μm).

After studying the behavior of the solvent mixtures, we found that addition of a small volume of a less volatile solvent such as cyclohexanone or ethylene glycol diethyl ether to the polymer solution produced more reproducible size distribution patterns. This was the reason why the membrane cocktail was prepared with the mixture of cyclohexanone and ethylene glycol diethyl ether. This can be explained if we assume that the solvent more miscible with water leaves the polymer first forming dispersed particles. Slower leaching of the second solvent from the polymer allowed the further particle ripening under milder conditions.

We were interested to find a parameter that would allow us to control the particle size in a continuous manner. To some extent, the dilution of the membrane cocktail provided such an instrument. We compared the size distribution patterns for three samples of the membrane cocktail diluted with THF in the range from 1:1 to 1:10. The size distribution of these microspheres is shown in Figure 2.5A. The dilutions 1:1, 1:5, and 1:10 produced the particles with an average diameter of 25 μm, 2 μm, and 200 nm. The 2 μm and 200 nm particles were further purified by filtering with Whatman no. 3 cellulose filters (pore size 6 μm) and a Whatman no. NL17 polyamide membrane (pore size 0.45 μm), respectively. The filtration allowed us to produce tighter distribution patterns. The distribution of filtered vs non-filtered particles is shown in Figure 2.5B.

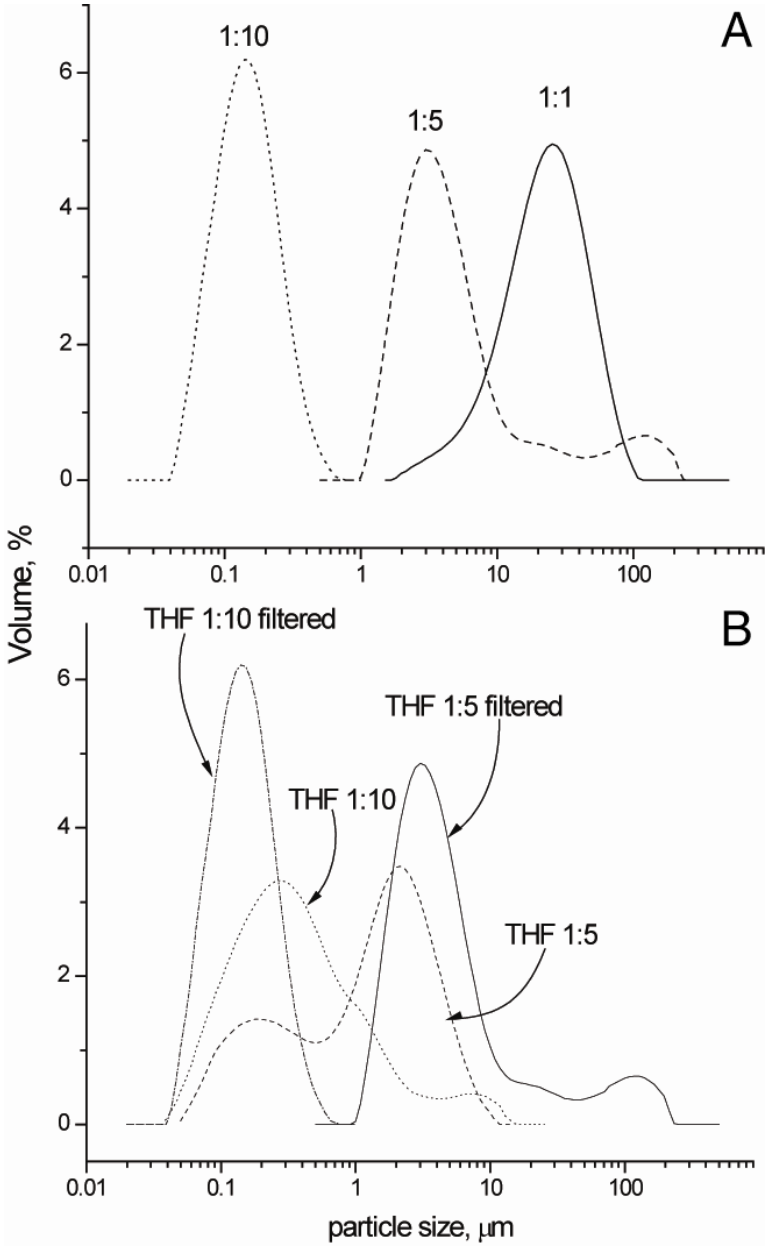

Figure 2.5. A) The effect of the polymer concentration in THF on the particle size distribution. The cocktail was diluted with THF (1:1, 1:5, and 1:10). The particles produced from 1:5 and 1:10 mixture were filtered with Whatman #3 cellulose filter (pore size 6 μm) and Whatman # NL17 polyamide membrane (pore size 0.45 μm) respectively. B) The size distribution of filtered vs. non-filtered particles produced from 1:5 and 1:10 mixtures.

Initially a choice of a surfactant was considered an important factor affecting the particle size distribution. Clearly, the surfactant stabilized the emulsion and facilitated the emulsification process reducing the amount of coagulum. Figure 2.6A shows a size distribution for four different surfactants BRIJ-35, PEG 5000, sodium dodecylsulfate, and Triton-X-100. Surprisingly, we found that a surfactant has little or no influence on the distribution pattern. The charged surfactant, sodium dodecylsulfonate, produced slightly larger variation in the distribution pattern than other neutral surfactants.

Moreover, the presence or absence of the micelles in the solution has apparently no effect on the distribution pattern. Figure 2.6B illustrated the results for two batches of particles obtained in the presence of Brij-35 in which the concentration was chosen below and beyond the CMC. The size deviation did not exceed a typical deviation between two identical batches of the particles. Apparently, the precipitation of the polymer does not take place inside the micelle in contrast to an emulsion polymerization process. This does not require a high concentration of the surfactant. A possibility to keep the surfactant concentration low is perhaps an important advantage. The emulsion of the sensor particles does not require additional separation steps such a surfactant removal, which is a critical step in emulsion polymerization.

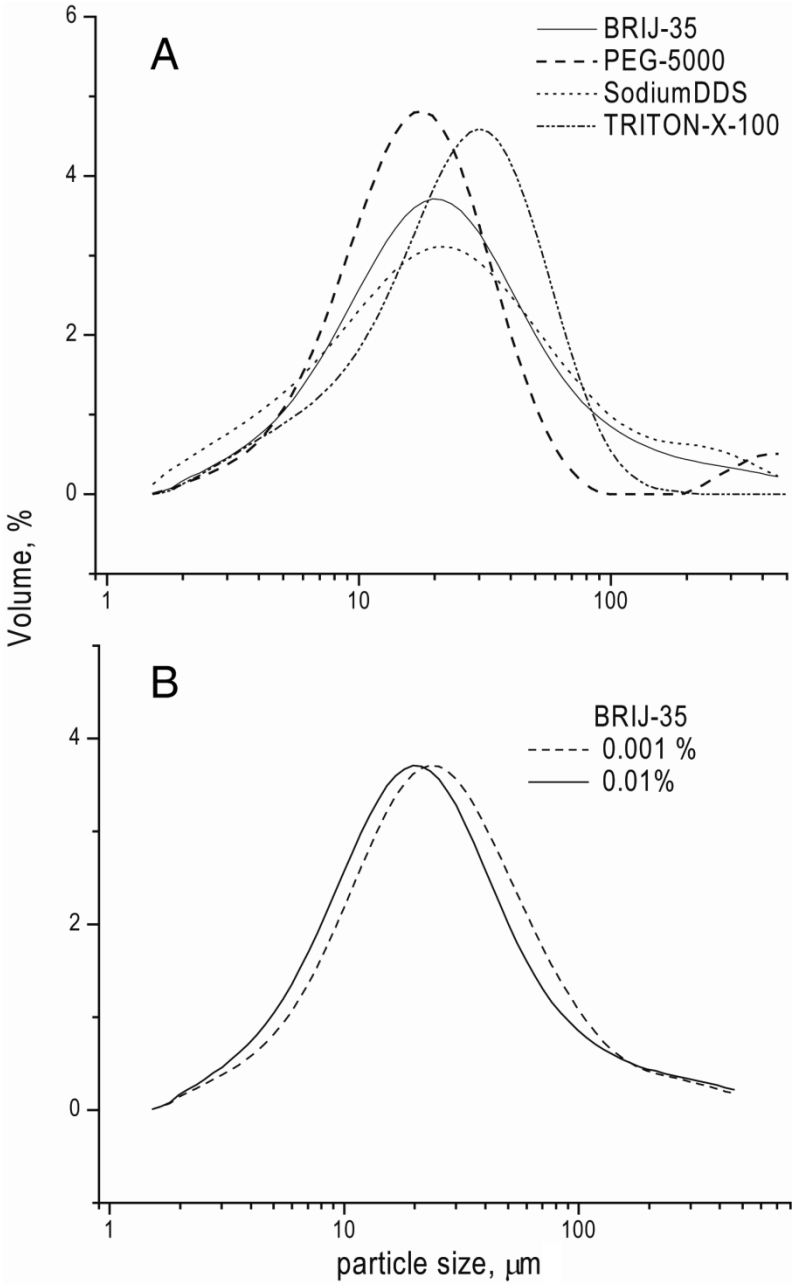

Figure 2.6. A) The role of the surfactant on the particle size distribution. The continuous phase contains 0.01% wt. of the surfactant. B) The effect of the concentration of the surfactant before and after CMC. The CMC of Brij-35 was $4.3 \cdot 10^{-5}$ M, 0.01 % and 0.001% wt. solutions correspond to $8.4 \cdot 10^{-5}$ M and $8.4 \cdot 10^{-6}$ M respectively.

We fabricated three different batches of ion-selective sensors using sodium ionophore X, BME-44, and ETH 5234 for sodium, potassium, and calcium optodes, respectively. Polymeric particles were obtained from a polymeric cocktail 1:1 diluted with THF. The average size of the particles was ~25-30 μm. However, for the calibration we selected the particles in which the diameter was 10 ± 1 μm. With an average exposure time of 300 ms, the signal from a single particle was 2500-3000 intensity units. This allowed us to obtain a reliable calibration for individual particles.

The calibration of three different types of ion optodes is shown in Figure 2.7. The degree of protonation (1 - α) was calculated using eq 2.2 and plotted as a function of the cation activity. The sodium-selective optodes at pH 7.0 showed a low detection limit of 5×10^{-4} M and a dynamic range of (5×10^{-4})-(5×10^{-1}) M. The experimental response was in excellent agreement with the theoretical response calculated according eq 2.1. The sensors demonstrated good reversibility and short response time.

Potassium and calcium optodes worked within (1×10^{-5})-(1×10^{-1}) M and (2×10^{-4})-(5×10^{-2}) M concentration range correspondingly. As it can be seen in parts A and B of Figure 2.7 at small cation activities, the value (1 - α), which is slightly smaller than unity, indicates an apparent incomplete protonation of the chromoionophore. The spectral patterns (not shown), however, were very similar to those we observed in 0.01 M solutions of HCl. This artifact is caused by a weak shoulder at 600-650 nm that was observed in buffered solutions. In a more acidic environment, which was used as a reference point for (1 - R), the shoulder disappeared. These deviations became considerably large only at low fluorescence intensities.

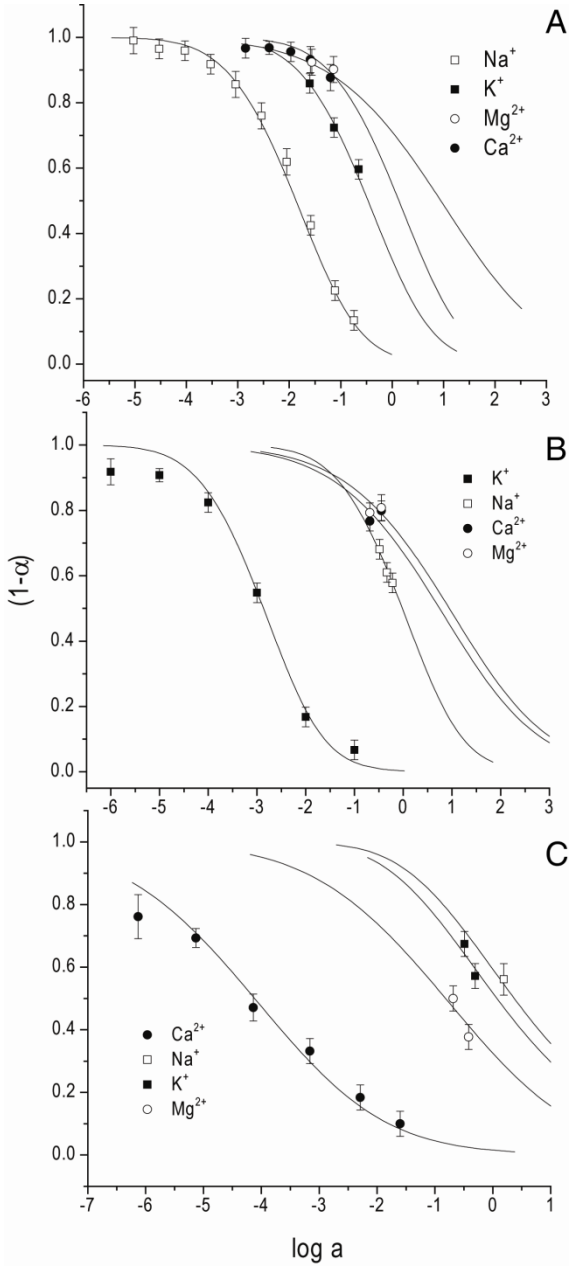

Figure 2.7. The optode responses for individual particles with respect to primary and interfering ions. The solutions contained 10 mmol of TRIS or MOPS buffers. A) sodium-selective optodes, the pH is 7.0 for sodium and 8.0 for the interfering ions. B) potassium-selective microspheres at pH 6.5, interfering ion measurement was taken at pH 7. C) calcium-selective optodes at pH 6.6.

The selectivity was calculated using the protocol described by Bakker.[2] The optodes demonstrated an excellent selectivity for the primary ions. The selectivity data are summarized in Table 2.1.

Table 2.1. The logarithms of selectivity coefficients ($\log K_{IJ}^{Opt}(SSM)$) for the ion optodes determined by the separate solution method.

	Interfering ions, $\log K_{IJ}^{Opt}(SSM)$		
	Na^+	K^+	Ca^{2+}
Primary ion			
Na^+	—	-3.4	-4.9
K^+	-2.4	—	-4.3
Ca^{2+}	-3.3	-4.2	—
Mg^{2+}	-2.8	-3.8	-3.3

2.5. Conclusions

We developed a very simple method for the fabrication of polymeric ion optodes. The solvent displacement method is a fast and reliable technique, which does not require additional preparation steps. Plasticized poly(vinyl chloride) along with the optode components was dissolved in a solvent miscible with water. Injection of a polymer solution into a stirred aqueous phase containing a surfactant caused spontaneous emulsification. The concentration of the polymer in the organic solvent and the choice of the solvent nature allowed us to control the particle size distribution within 200 nm-30 μm. The size distribution was reproducible with a moderate degree of monodispersity. The concentration and the nature of the surfactant had a little effect on the particle size distribution. Ion optodes selective for sodium, potassium, and calcium cations were prepared and calibrated using

chromoionophore I, lipophilic ion-exchanger and sodium ionophore X, BME-44, and ETH 5234 for sodium, potassium, and calcium optodes, respectively. The sensors were fully functional with excellent selectivity to interfering ions.

2.6. Acknowledgement

The authors acknowledge the Office of Naval Research and Oregon Nanoscience and Microtechnologies Institute for financial support of this research through ONAMI's Nanoelectronics and Nanometrology Initiative.

2.7. References.

(1) Buhlmann, P.; Pretsch, E.; Bakker, E. *Chem. Rev.* **1998**, *98*, 1593-1687.

(2) Bakker, E.; Buhlmann, P.; Pretsch, E. *Chem. Rev.* **1997**, *97*, 3083-3132.

(3) Morf, W. E.; Seiler, K.; Rusterholz, B.; Simon, W. *Anal. Chem.* **1990**, *62*, 738.

(4) Shortreed, M.; Bakker, E.; Kopelman, R. *Anal. Chem.* **1996**, *68*, 2656-2662.

(5) Kellar, K. L.; Iannone, M. A. *Experimental Hematology* **2002**, *30*, 1227-1237.

(6) Vignali, D. A. A. *Journal of Immunological Methods* **2000**, *243*, 243-255.

(7) Dickinson, T. A.; Michael, K. L.; Kauer, J. S.; Walt, D. R. *Anal. Chem.* **1999**, *71*, 2192-2198.

(8) Fulton, R. J.; McDade, R. L.; Smith, P. L.; Kienker, L. J.; Kettman, J. R. J. *Clin.Chem.* **1997**, *43*, 1749-1756.

(9) Oleschuk, R. D.; Shultz-Lockyear, L. L.; Ning, Y.; Harrison, D. J. *Anal. Chem.* **2000**, *72*, 585-590.

(10) Buck, S. M.; Koo, Y. E. L.; Park, E.; Xu, H.; Philbert, M. A.; Brasuel, M. A.; Kopelman, R. *Current Opinion In Chemical Biology* **2004**, *8*, 540-546.

(11) Buck, S. M.; Xu, H.; Brasuel, M.; Philbert, M. A.; Kopelman, R. *Talanta* **2004**, *63*, 41-59.

(12) Telting-Diaz, M.; Bakker, E. *Anal. Chem.* **2002**, *74*, 5251-5256.

(13) Tsagkatakis, I.; Peper, S.; R, R.; Bell, M.; Bakker, E. *Anal. Chem.* **2001**, *73*, 6083-6087.

(14) Wygladacz, K.; Bakker, E. *Anal. Chim. Acta.* **2005**, *532*, 61-69.

(15) Tseng, C. M.; Lu, Y. Y.; El-Aasser, M. S.; Vanderhoff, J. W. *Journal of Polymer Science Part A: Polymer Chemistry* **1986**, *24*, 2995-3007.

(16) Peper, S.; Tsagkatakis, I.; Bakker, E. *Anal. Chim. Acta.* **2001**, *442*, 25-33.

(17) Clark, H. A.; Hoyer, M.; Philbert, M. A.; Kopelman, R. *Anal. Chem.* **1999**, *71*, 4831-4836.

(18) Chu, B. S.; Ichikawa, S.; Kanafusa, S.; Nakajima, M. *J. Agric. Food Chem.* **2007**, *55*, 6754-6760.

(19) Reis, C. P.; Neufeld, R. J.; Ribeiro, A. J.; Veiga, F. *Nanomed.* **2006**, *2*, 8-21.

(20) Ribeiro, H. S.; Chu, B.-S.; Ichikawa, S.; Nakajima, M. *Food Hydrocolloids* **2008**, *22*, 12-17.

(21) Meier, P. C. *Anal. Chim. Acta* **1982**, *136*, 363.

CHAPTER 3

SURFACE AREA EFFECTS ON THE RESPONSE MECHANISM OF ION OPTODES: A PRELIMINARY STUDY

Valeriya Bychkova, Alexey Shvarev

Analytical Chemistry

American Chemical Society

1155 16th Street N.W., Washington, DC 20036

Volume 81(**2009**), Issue 17, 7416–7419

3.1. Abstract

The relationship between the surface-to-volume ratio and the response mechanism of polymeric ion probes (ion optodes) is not well understood. In this work, the surface-to-volume ratio of ion optodes was systematically increased in an attempt to characterize this relationship. Several different batches of ion-selective optodes were fabricated via the solvent displacement method using sodium ionophore X, BME-44, and ETH 1001 for sodium-,potassium-, and calcium-selective optodes, respectively. Dilution of the membrane cocktail with varying amounts of an organic solvent provided a convenient tool to control the resulting particle size distribution. Specifically, ion optodes of five different size distributions were fabricated. An apparent shift of the response function on the pH scale was observed for optodes with identical composition that differed in terms of size. There was a strong correlation between the calculated specific surface area and the apparent ion-exchange constant for all three types of ion optodes. However, there was an indication that selectivity does not substantially correlate with the optode size. We hypothesize that the observed effect is caused by surface phenomena which contribute to the overall optode response. The results reported here may raise a word of caution about the application of established response models, which were developed for macroscopic ion optodes, toward probes at micrometer and submicrometer scales.

3.2. Introduction

All existing life forms rely on the delicate balance between intracellular and extracellular electrolytes. Ion-selective electrodes (ISE's) are widely used for the detection of physiologically important ions such as H^+, Na^+, K^+, Ca^{2+}, and Cl^-.[1] Ion-selective electrodes measure free ion activities, contrary to fluorescence methods, which measure total ion concentrations. As a result, in the detection of

physiological electrolytes, ISE's constitute a complementary methodology to fluorescence techniques.

Recently, the fluorescence microscope has replaced the classical transmission microscope as the most widely used instrument in cell biology. Imaging microspectrometry, which allows one to perform "chemical mapping", became a very affordable technique due to continuous progress in charge-coupled device (CCD) imagers, compact spectrometers, and piezoelectric positioners.

There is a growing interest in the detection of physiological electrolytes with fluorescence microscopy using ion-selective polymeric optical sensors.[2-5] Fluorescence microscopy can be easily combined with miniature optical ion probes with only minor modifications to the existing experimental setup. Microsphere ion optodes can be fabricated within a size range of 50 nm to 50 μm using emulsion[2,6] and dispersion[7] polymerization.

Recently, we described the fabrication of micrometer- and submicrometer-sized optodes via solvent displacement method.[8] Briefly, poly(vinyl chloride) (PVC) and plasticizer along with the sensing components were dissolved in the solvent miscible with water. The solution was injected into the aqueous phase containing a small concentration of a surfactant. Polymer precipitation following the solvent displacement instantaneously produced an emulsion of spherical particles. The feasibility of this method was demonstrated by the fabrication of fully functional sodium, potassium, and calcium optodes. Therefore, ion probes can be used to monitor ionic activities and, applying imaging processing methods, ionic fluxes in intracellular and extracellular environments.

The response mechanism of an ion optode is based on the ion-exchange equilibrium in the two-phase (sample/optode) system.[1,9] Thus, the ion optode is always reconditioned if the composition of the sample is changed. The reconditioning is necessary in order to achieve chemical equilibrium in two-

phase sample/optode system. On the contrary, the ISE response is described as an "interfacial" phenomenon. After a short period of equilibration at the phase boundary, no significant ion transport takes place in the membrane bulk. Therefore, optodes are usually referred as "bulk" sensors in contrast to their interfacial counterparts, ISE's.

We may assume reasonably that local physicochemical properties at the surface may be different from that in the bulk. A simple calculation reveals that a typical polymeric pH-selective optode, approximately 200 nm in diameter and containing the chromoionophore ETH 5294, contains ca. 3000 molecules of ETH 5294. An optode which is 4 times smaller (50 nm in diameter) will have a higher surface-to-volume ratio and will contain only 200 chromoionophore molecules. A certain fraction of the optode components will be located on the optode surface at the sensor/sample interface. Thus, as the size of an ion optode decreases and surface-to-volume ratio increases, we may expect that interface processes will eventually contribute to the optode response. This phenomenon has yet to be explored. We report here on the possible effects of an increasing surface-to-volume ratio on the response of polymeric ion probes.

3.3. Experimental section

3.3.1. Reagents.

High molecular weight PVC, bis(2-ethylhexyl) sebacate (DOS), *tert*-butyl calix[4]arene tetraethyl ester (sodium ionophore X), 2-dodecyl-2-methyl-1,3-propanediyl bis[*N*-[5′-nitro(benzo-15-crown-5)-4′-yl]carbamate] (BME-44, potassium ionophore), diethyl *N*,*N*′-[(4*R*,5*R*)-4,5-dimethyl-1,8-dioxo-3,6-dioxaoctamethylene] bis(12-methylaminododecanoate) (ETH 1001, calcium ionophore I), sodium tetrakis[3,5-bis(trifluoromethyl)phenyl borate(NaTFPB), 9-

(diethylamino)-5-octadecanoylimino-5*H*-benzo-[*a*]phenoxazine (chromoionophore I, ETH 5294), tetrahydrofuran (THF), cyclohexanone, ethylene glycol diethyl ether, polyoxyethylene (23) lauryl ether (Brij-35), and 3-(*N*-morpholino)propanesulfonic acid (MOPS) were from Aldrich (Milwaukee, WI). All other chemicals were purchased from VWR (West Chester, PA). Aqueous solutions were prepared by dissolving the appropriate salts in deionized water (18.2 MΩ cm).

3.3.2. Preparation of membrane cocktail.

The sensor components, the polymer (PVC), and the plasticizer (DOS) were dissolved in 1 mL of a 2:1 mixture of cyclohexanone and ethylene glycol diethyl ether. Specifically, the sodium-selective cocktail contained 40 mmol/kg sodium ionophore X, 20 mmol/kg ion-exchanger NaTFPB, and 10 mmol/kg chromoionophore I. The potassium-selective cocktail contained 30 mmol/kg BME-44, 15 mmol/kg NaTFPB, and 7.5 mmol/kg chromoionophore I. The composition of calcium-selective cocktail consisted of 22 mmol/kg calcium ionophore I, 7 mmol/kg ion-exchanger NaTFPB, and 4.5 mmol/kg chromoionophore I. THF was added to dilute the dissolved polymer solution in the range from 1:1 to 1:10.

3.3.3. Fabrication of the optode beads.

A small (~8 mL) vial was filled with a 0.01 wt % Brij-35 solution in deionized water. A small amount of the polymer solution was injected rapidly into a stirred aqueous solution of the surfactant. The emulsion was filtered then, and the filtrate was used to prepare all working solutions. A more detailed description of

the fabrication procedure, particle characterization, and optode response mechanism can be found in Appendices A and B.

3.3.4. Instrumentation.

The experimental setup consisted of an inverted fluorescence microscope and an imaging spectrometer with a CCD camera. Fluorescence of the chromoionophore was caused by excitation at 535 (±25) nm and recorded from 600 to 800 nm. A xenon arc lamp with a four-filter fast wavelength switch was employed as a light source. Ratiometric fluorescence measurements were performed comparing emission peaks at 650 and 680 nm. A more detailed description of the instrumentation used is available in Appendices A and B.

3.4. Results and discussion

Recently we reported on a simple method for the fabrication of polymeric ion optodes based on a solvent displacement process.[8] We were able to control the particle size distribution within 200 nm to 30 μm due to alterations in the concentration of the polymer in the organic solvent and judicious choice of the solvents. Although the solvent composition gave us a "coarse" control over a particle size distribution, the concentration of a polymer in the membrane cocktail served as a "fine" tool. To some extent, this allowed us to change the size distribution in a continuous manner.

Figure 3.1 shows the resulting size distribution of polymeric beads corresponding to a series of continuous dilutions of the initial membrane cocktail with THF. The size distribution for the 1:1 dilution is not shown because the relatively large size of the optode spheres allowed us to determine the bead diameter with a

microscope and manually select spheres which were 10 ±1 μm in diameter. Dilutions of 1:5, 1:7, 1:8, and 1:10 yielded microspheres with size distribution maxima at 1.80, 0.50, 0.27, and 0.18 μm, respectively.

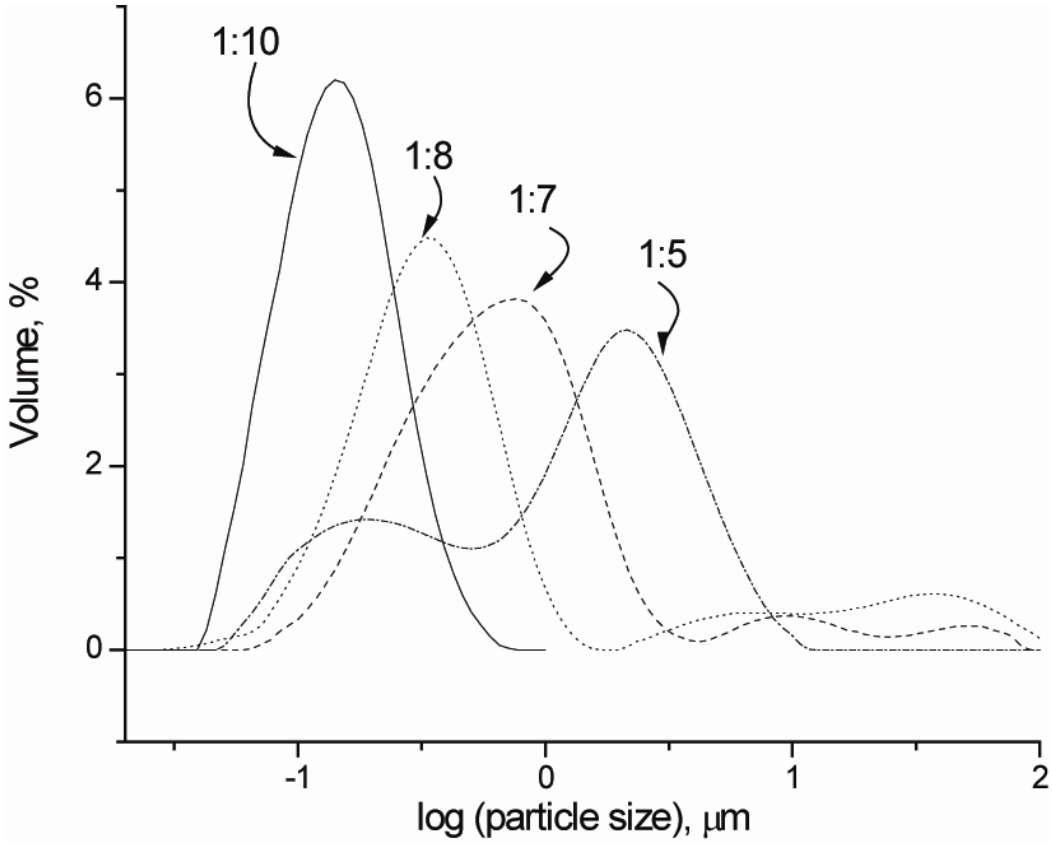

Figure 3.1. Effect of polymer concentration in THF on particle size distributions. The membrane cocktail was diluted with THF (1:5, 1:7, 1:8, and 1:10). The emulsions obtained were filtered using Whatman no. 3 cellulose filters (pore size 6 μm), glass microfiber filters GF/D (pore size 2.7 μm), glass microfiber filters GF/B (pore size 1.0 μm) and a Whatman no. NL17 polyamide membrane (pore size 0.45 μm), respectively.

Ion-selective optodes selective for sodium, potassium, and calcium were fabricated. Five dilutions of the various membrane cocktails were made,

according to the dilution scheme mentioned above. The membrane cocktails contained a lipophilic ion-exchanger and, depending on the ion the optode was selective for, one of the following: sodium ionophore X, BME-44, or ETH 1001, respectively. In order to test the functionality of the ion optodes, calibration curves were collected with respect to the activity of the primary ion in 10 mM TRIS and in 10 mM MOPS buffer solutions.

Initially, a TRIS buffer, adjusted to pH 7.5, was used to check the sodium-selective optodes' response to sodium ions. We noticed that, whereas relatively large (10 μm) ion probes behaved like the optode films of macroscopic size, the complete protonation of smallest ion probes cannot be achieved at pH 7.5. This can be easily seen in the spectra where the fraction of the protonated form of the chromoionophore (1 - R) did not exceed 0.6-0.7 units. The protonation degree was approximately 0.7 in the blank solution (in complete absence of the primary ion). However, if the pH was reduced to 6.5 using the MOPS buffer, the entire calibration curve was restored. Apparently, although all of the experimental parameters were kept constant, smaller sodium-selective ion optodes required more acidic pH in order to reach the same response function. This contradicts previously reported data,[2,6] collected using poly(decyl methacrylate)-based (PDMA) ion optodes, which demonstrated that small system sizes had little or no effect on the optode calibration. In the present work, the apparent pH bias was observed for sodium, potassium, and calcium-selective optodes.

In order to further explore this effect, we studied the optode response as a function of pH at fixed activities of the primary ions. The resulting calibration curves are shown in Figure 3.2 for two batches of sodium- and potassium-selective particles with size distribution maxima at 10 μm and 180 nm. In contrast to the sodium-selective optodes, a basic shift in pH was observed for the potassium-selective optodes when comparing the calibration curves for the two different optode size distributions (Figure 3.2B).

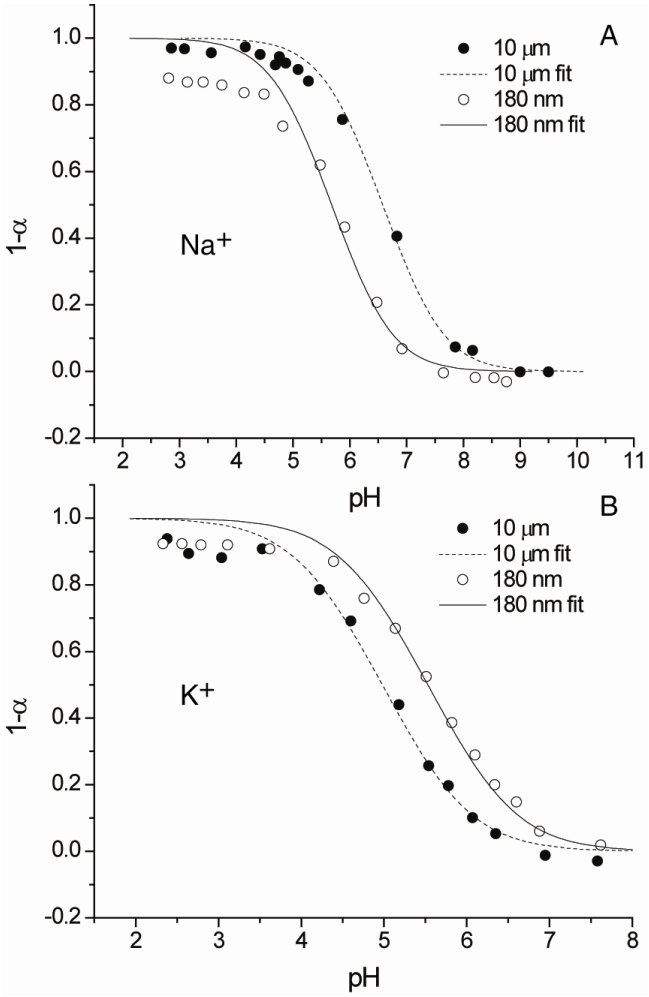

Figure 3.2. Optode response for individual particles (10 ± 1 µm in diameter) and emulsions with an average particle size of 0.18 µm with respect to pH. The solutions contained 3.3 mM of citric acid, 5.5 mM of boric acid and 5.0 mM of phosphoric acid, and the concentration of the primary ion was kept at 50 mM. The calibration curve for the emulsion shifted by 0.6 pH units to a more acidic pH when compared to the 10 ± 1 µm microsphere response for sodium-selective optodes (A). The pH shift of the calibration curve for the emulsion was 0.9 units towards a more basic pH when compared to the 10 ± 1 µm microsphere response for potassium-selective optodes (B). Please, note that the scales on the x-axis are different for these two plots.

The resulting pH bias reached 0.6 pH units for the sodium-selective and 0.9 pH units for potassium-selective probes. This is a substantial bias when compared to the total working range of the optodes, which is 3 pH units.

According to eq 3.1, the optode response (expressed as a mole fraction of unprotonated chromoionophore, *R*) depends on the following parameters: the ion-exchange constant K_{exch}, activities of cation I^{z+} and hydrogen in the aqueous phase, a_I and a_H, respectively, and the total concentrations of ionophore (*L*), ion-exchanger (*R*), and chromoionophore (*Ind*).[1]

$$a_I = (z_I K_{exch})^{-1} \left(\frac{\alpha}{1-\alpha} a_H\right)^{z_I} \left(\frac{R_T - (1-\alpha) Ind_T}{\left\{ L_T - (R_T - (1-\alpha) Ind_T) \left(\frac{n_I}{z_I}\right) \right\}^{n_I}} \right) \quad (3.1)$$

If we assume that the compositions of particles of different sizes are practically identical, the only "variable" is the apparent ion-exchange constant K_{exch}.

The value of the ion-exchange constant K_{exch} was calculated using eq 3.1 in order to plot the best fit for the sigmoidal optode response function (Figure 3.2). In Figure 3.3 the resulting values of log K_{exch} are shown as a function of the specific surface area of ion probes that corresponds to the size distribution maximum. The density of the PVC matrix was 1.0 g/cm^3. The log-log graphs are practically linear with correlation coefficients of 0.99 or better. However, for clarity, the plots in Figure 3.3 are shown in semilogarithmic coordinates demonstrating asymptotic behavior of the relationship between the ion-exchange constant and the specific surface area. The results were fit with the logarithmic decay $y = a - b(\ln(x + c))$. As can be seen, the resulting bias of the ion-exchange constant is quite substantial (~0.7-0.8) for singly charged ions. For calcium, the value of K_{exch} is much less affected by this effect. The resulting shift of the calibration curve is very reproducible.

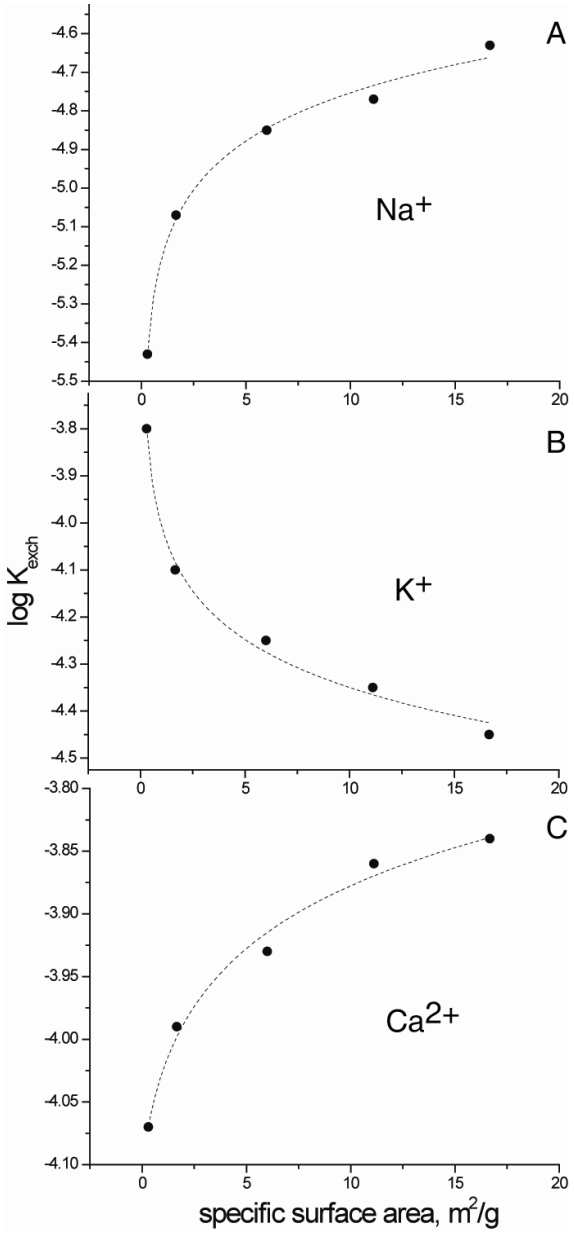

Figure 3.3. The relationship between log K_{exch} and specific surface area. The K_{exch} was obtained from the pH response of the single particles (10 ± 1 µm in diameter) and filtered emulsions produced using membrane cocktails diluted with THF (1:5, 1:7, 1:8, and 1:10). The specific surface area of ion probes in the form of emulsions corresponds to the size distribution maximum for (A) sodium-selective optodes, (B) potassium-selective optodes, and (C) calcium selective optodes.

The ion-exchange constant is a function of the relative lipophilicities (k_I and k_H) of metal ion I^{z+} and proton H^+, respectively, the stability constant β_{ILn} for the ion-ionophore complex, and the acidity constant K_a of the chromoionophore. The variables β_{ILn} and K_a are defined for the organic phase.

$$K_{exch} = \left(\frac{K_a}{k_H}\right)^z k_I \beta_{IL_n} \tag{3.2}$$

The selectivity of ion-selective optodes as well as ISE's is directly related to the relative lipophilicity of the primary and interfering ions and stability constant of the appropriate ion-ionophore complexes.

We expected that the specific surface area of the ion optodes would affect the selectivity. The selectivity was measured using the separate solution method and calculated according to known protocol.[1] The resulting selectivity coefficients are shown in Table 3.1. Apparently, there is no direct correlation between the size of ion probes and the selectivity.

Table 3.1. Logarithm of selectivity coefficients ($\log K_{IJ}^{Opt}(SSM)$) for sodium-selective ion optodes.[a]

Specific surface area, $m^2\ g^{-1}$	Interfering ions, $\log K_{IJ}^{Opt}(SSM)$		
	K^+	Mg^{2+}	Ca^{2+}
0.3	-2.4	-2.8	-3.3
1.7	-2.8	-3.8	-3.7
6.0	-2.6	-3.3	-3.2
11.1	-2.6	-2.8	-2.8
16.7	-2.5	-2.9	-2.9

[a] Selectivity coefficients were determined by the separate solution method (SSM) with respect to the specific surface area of ion probes that corresponded to the size distribution maxima.

This suggests one of several possible explanations for the observed bias. As the size of an ion optode decreases, we may expect that interface processes will eventually contribute to the optode response. Specifically, if the optode composition, relative lipophilicities of the metal ions and protons, and the stability constant of the ion-ionophore complex remain constant, the local surface pH, and consequently the K_a of the chromoionophore, may be affected by the surface potential. Indeed, the deviation of the interfacial acidity from that in the phase bulk is a very well-known fact. This deviation of the acid-base equilibrium has been studied extensively at the liquid/liquid[10] and gas/liquid[11,12] interfaces.

The results reported here may be an important indication that the response models, developed for the macroscopic ion optodes, cannot be easily applied to the probes at micrometer and submicrometer scale. If the size of the probe is comparable to the thickness of diffusion part of the electrical double layer and

the specific surface area exceeds several square meters per gram, the surface terms may overwhelm the bulk. In this case, we can no longer use the term “bulk” optodes. Moreover, in a complex, highly heterogeneous environment, such as an intracellular domain, the response and the calibration of the probe may be affected by highly localized phenomena. Nevertheless, this effect requires further investigation, which is currently in progress in our lab.

3.5. Conclusion

A solvent displacement method is a convenient tool, which allowed us to fabricate several different batches of ion-selective optodes using a lipophilic ion-exchanger and sodium ionophore X, BME-44, and ETH 1001 for sodium, potassium, and calcium optodes, respectively. The optode batches had identical chemical compositions but were different in terms of size distribution.

Depending on the size for the ion optodes of the same chemical composition we observed an apparent shift of the response function on the pH scale. This bias clearly can be seen for sodium, potassium, and calcium optodes if the activity of the primary ion remains constant and the response is plotted as a function of the pH. There is a strong correlation between a calculated specific surface area and the apparent ion-exchange constant for all three types of the probes. In contrast, the selectivity does not substantially correlate with the optode size. The observed effect is possibly caused by the surface phenomena contributing to the overall optode response.

3.6. Acknoweldgement

The authors acknowledge the Office of Naval Research and the Oregon Nanoscience and Microtechnologies Institute for financial support of this research through ONAMI's Nanoelectronics and Nanometrology Initiative.

3.7. References.

(1) Bakker, E.; Buhlmann, P.; Pretsch, *E. Chem. Rev.* **1997**, *97*, 3083-3132.

(2) Buck, S. M.; Koo, Y. E. L.; Park, E.; Xu, H.; Philbert, M. A.; Brasuel, M. A.; Kopelman, R. *Current Opinion In Chemical Biology* **2004**, *8*, 540-546.

(3) Clark, H. A.; Hoyer, M.; Philbert, M. A.; Kopelman, R. *Anal. Chem.* **1999**, *71*, 4831-4836.

(4) Dubach, J. M.; Harjes, D. I.; Clark, H. A. *J. of the Am. Chem. Soc.* **2007**, *129*, 8418-8419.

(5) Kurihara, K.; Ohtsu, M.; Yoshida, T.; Abe, T.; Hisamoto, H.; Suzuki, K. *Anal. Chem.* **1999**, *71*, 3558-3566.

(6) Buck, S. M.; Xu, H.; Brasuel, M.; Philbert, M. A.; Kopelman, R. *Talanta* **2004**, *63*, 41-59.

(7) Peper, S.; Tsagkatakis, I.; Bakker, E. *Anal. Chim. Acta.* **2001**, *442*, 25-33.

(8) Bychkova, V.; Shvarev, A. *Anal. Chem.* **2009**, *81*, 2325-2331.

(9) Buhlmann, P.; Pretsch, E.; Bakker, *E. Chem. Rev.* **1998**, *98*, 1593-1687.

(10) Naujok, R. R.; Paul, H. J.; Corn, R. M. *J. Phys. Chem.* **1996**, *100*, 10497-10507.

(11) Tamburello-Luca, A. A.; Hebert, P.; Antoine, R.; Brevet, P. F.; Girault, H. H. *Langmuir* **1997**, *13*, 4428-4434.

(12) Zhao, X.; Subrahmanyan, S.; Eisenthal, K. B. *Chem. Phys. Lett.* **1990**, *171*, 558-562.

CHAPTER 4

QUANTUM DOTS DOPED ION-SELECTIVE OPTODES BASED ON THE INNER FILTER EFFECT

Valeriya Bychkova, Nataliia Pylypiuk, Vincent Remcho, Alexey Shvarev, James D. Ingle, Jr.*

To be submitted

4.1. Abstract

The unique optical properties of quantum dots (QDs) were utilized to develop improved ion-optodes based on the inner filter effect (IFE) - a promising and versatile tool in biochemical determination of physiological electrolytes. IFE based, ion-optodes were in the form of spherical particles with sensing components were fabricated with a solvent displacement method, a simple, single-step method. Two types of QDs were incorporated into the particles and acted as excitation sources for the chromoionophore, ETH 5294, providing a "soft" excitation. The fluorescence from two different types of QDs was monitored. The attenuation of the fluorescence signals by the protonated and unprotonated form of the ionophore was used to determine the degree of protonation. The incapsulation of QDs in polymeric spheres improves their stability over a wider pH range and did not interfere with the responsivity of the ion-optode sensing components. The particles (10 ± 1 μm) provide an excellent response to primary metal-ion and pH. The dynamic range was 0.1 mM – 0.1 M at pH 7.5 and pH 6.0 – 8.5 at 0.01 M Na^+. With submicron particles, the ζ-potential increased slightly with QDs introduction assuming positive net charge possessed by CdSe QDs and their location on the optode particle surface.

4.2. Introduction

Quantum dots (QDs) are colloidal, nanocrystalline semiconductors identified as a special class of nanoparticles due to their novel, fluorescence characteristics. Their unique optical properties have led to their use for fluorescent labeling[1-4] and bioimaging[5-7]. Compared to conventional organic fluorophores, QDs have narrow emission spectra and broad absorption spectra[8]. These properties allow QDs of different sizes (and thus with different emission wavelength maxima) to be excited with a single excitation source[9]. Moreover, QDs are more resistant to

optical signal degradation during excitation (e.g., photobleaching)., which enables applications where longer imaging time is necessary. Typically in microfluorometry, a very high irradiance excitation source is required to excite a fluorophore. Complete photobleaching of organic dyes can occur in 10 s or less of constant illumination.

The wide range of emission maxima of different QDs has made it possible the use of nanocrystals as excitation donors in photochemically-induced fluorescence[10]. Coupled with the broad absorption spectra typical of QDs, excitation of organic dyes (acceptor) is possible in situations where direct excitation is forbidden or not preferable[11]. Two known phenomena have been utilized for this purpose.

Förster Resonance Energy Transfer (FRET) is a non-radiative energy transfer between two molecules or two parts of one molecule that are separated from each other by a distance that is greater than the sum of their van der Waals radii. FRET from donor QDs to acceptor dyes is strongly dependent on the center-to-center separation distance, the number of acceptor dye molecules per QD, the spectral overlap between QD emission and acceptor absorption, etc. Systematic studies have examined the quantitative relationships between these factors and the FRET efficiency[12].

By adding organic coatings to QDs, it is possible to tailor nanocrystals to meet specific FRET requirements. This work has led to the creation of a wide variety of sensors where QDs serve as an architectural support for conjugating analyte-selective ligands. When a binding event occurs, a quantitative change in the photoluminescence signal of the QD results. Sensors that utilize this approach have been reported for the multiplexed analysis of DNA hybridization events[13], as well as for the chemical detection of cyanide[14]. Recently, Wang et al.[15] reported a silica-based, nanosphere, ratiometric sensor (ANSor) for local pH-

monitoring. Water-soluble QDs were used as donors in sodium sensors to measure sodium activities from 0 nM to 130 nM in solutions[16].

An alternative approach to FRET is to utilize the inner filter effect (IFE). This phenomenon is based on the attenuation of the emission signal due to the absorption of emitted photons by another molecule. The IFE differs from FRET in that the two species involved in the energy exchange are not necessarily attached to each other, but simply co-exist in the sensing medium. Tohda et al.[17] utilized IFE to detect non-fluorescent (but absorbing) molecules using fluorescent organic dyes as energy donors. Dubach et al.[18] demonstrated the possibility of incorporating QDs into the polymer matrix of ion-selective sensors together with a fluorescent dye, and utilized IFE for signal detection. In this case the fluorophore absorbed the light emitted from QDs, thus the attenuation of QD fluorescence signal served as an indirect measurement of ion activity in the solution that contacted with an optode sensing film. Ruedas-Rama et al.[19] reported CdSe/ZnS photoluminescence lifetime-based nanosensors with a linear pH response in the range of 5.2 – 6.9 that can be used in intracellular media. A similar sensor was built for monitoring of sodium from 0.1 mM to 0.1 M at pH 4.8[20].

Here we report a facile method for preparing QD-doped ion optodes based on a chromoionophore in spherical form with tunable size. Uniquely, two absorption bands of the chromoionophore were used to enable a ratiometric measurement. Two sizes of QDs with different emission wavelength maxima (to match the two absorbance maxima of the dye) were incorporated. This approach allowed the measurement of the attenuation of the emission (caused by the sensor dye) from two separate QDs with a single light source. The polymeric sensors were fabricated via solvent displacement method. These new sensors combine the properties of a “traditional” ion-selective optodes and the IFE to yield a more effective and stable measurement tool. Each measurement was made on a single

particle with an inverted fluorescence microscope and an imaging spectrometer with a CCD camera.

4.3. Experimental section

4.3.1. Reagents.

9-(diethylamino)-5-octadecanoylimino-5H-benzo[α]phenoxazine (chromoionophore I or ETH 5294), tert-butyl calix[4]arenetetraehyl ester (sodium ionophore X), potassium tetrakis(4-chlorophenyl) borate (KTCPB), high molecular weight poly(vinyl chloride) (PVC), bis(2-ethylhexyl) sebacate (DOS), polyoxyethylene (23) lauryl ether (Brij-35), tetrahydrofuran (THF), cyclohexanone, acetone, ethylene glycol diethyl ether (EGDE), 1-decanethiol (1-DCT), tris(hydroxymethyl)aminomethane (TRIS), and 3-(N-Morpholino) propanesulfonic acid (MOPS) were purchased from Sigma – Aldrich (Milwaukee, WI). The core-shell Qdot® 545/605/655 ITK™ (QD545, QD605, and QD655, respectively), 1 µM solution in decane, were purchased from Invitrogen (Eugene, OR). All other chemicals were purchased from VWR (West Chester, PA). All aqueous solutions were prepared in deionized water (18.2 MΩ cm; Millipore, Milli-Q Water Systems).

4.3.2. Membrane cocktail preparation.

The membrane cocktail contained sensing components, polymer, and plasticizer dissolved in a solvent. The concentration of the sensing components was 5 mmol/kg chromoionophore I (ETH5294), 10 mmol/kg ion-exchanger KTCPB, 20 mmol/kg sodium ionophore X, 15 µmol/kg QD545 and 2.5 µmol/kg QD605. The membrane was made with 33% (w/w) polymer (PVC) and 66% plasticizer

(DOS). The sensing components, polymer and plasticizer were dissolved in 1 mL of a 2:1(v/v) mixture of cyclohexanone and EGDE and shaken vigorously for 2 hr to achieve homogeneity.

4.3.3. Fabrication of polymer films and polymeric beads.

A 70-µL aliquot of the membrane cocktail was spin-coated at 250 rpm for 2 min on a 22x22 mm microscope coverslip. The films were covered, allowed to dry, and then conditioned at pH 7 for 1 hr.

The solvent displacement method was used for optode fabrication[21]. THF was added to dilute the polymer solution in a 1:1 ratio. A small amount of this mixture was rapidly injected with a syringe into stirred 0.01% (w/w) Brij-35 aqueous solution. Polymer precipitation following the solvent displacement instantaneously produced an emulsion of spherical particles. The emulsion was filtered with a Whatman no. 1 filter; the filtrate was collected and stored in a vial.

4.3.4. Instrumentation.

The zeta-potential of polymeric sensor particless of different composition was measured with phase analysis light scattering (PALS). All measurements were carried out using ZetaPALS ζ-potential analyzer (Brookhaven Instruments Corporation, Holtsville, NY). Samples contained 3 mM NaCl at pH 7.

Fluorescence measurements were made with an inverted fluorescence microscope and an imaging spectrometer with a CCD camera. A xenon arc lamp was employed as a light source. The quantum dots were excited in the wavelength range at 350 ± 25 nm as defined by an interference filter. The fluorescence signal of the QDS and chromophore was observed from 500 to

700 nm. For final calculations, the ratio of the fluorescence signal at 545 nm to that at a 605 nm was calculated.

The pH of the solutions was maintained with 10 mM TRIS and MOPS buffers, and a universal buffer solution containing 3.3 mM citric acid, 5.5 mM boric acid and 5.0 mM phosphoric acid adjusted with 1 M KOH. All experiments were conducted at ambient temperature (23 ± 2 °C). Activity coefficients were calculated according to Debye-Hückel formalism[22]. The instrumentation used and optode response calculation is described in more detail in Appendices A and C.

4.4. Results and discussion

Normally the absorbance of common chromoionophores cannot be monitored in small sensing beads because the path length is too small. However, when the chromoionophore is fluorescent, the degree of protonation can be monitored.[21] Direct excitation of the fluorophore has been employed for sensing purposes, but photobleaching of the dye or fluorophore becomes an issue with continuous exposure to excitation radiation.

In this study the absorption characteristics of the chromoionophore can be monitored in beads because QDs can be excited in the region where the dye has no appreciable absorbance. The degree of protonation of the chromoionophore can be determined by the attenuation of the QD fluorescence by the chromoionophore. Hence the chromoionophore is exposed to much softer excitation conditions than normal because the irradiance of the QD fluorescence is an extremely small fraction of the excitation source irradiance.

One possible drawback of the scheme described above is the inability to simultaneously monitor both the protonated and unprotonated forms of the

chromoionophore. To overcome this limitation, two types of QDs that match two absorption bands (protonated and unprotonated) of the chromoionophore were incorporated into the sensor. This approach allows measurement of the attenuation of emission quenching (caused by the dye) from two separate QDs with one excitation source. Use of the ratio as the analytical signal is advantageous because the ratio is independent of variations in conditions that affect the absolute emission intensity of both QDs by the same proportion such as the light source intensity or the particle size; it is not affected by excitation and emission light scattering and depends only on the degree of the chromoionophore protonation.

The spectra in Figure 4.1 illustrate the overlap of the emission spectra of the QDs and the absorption spectra of the chromoionophore. The deprotonated form of ETH 5294 exhibits an absorption maximum at 536 nm, while the protonated form has two absorption maxima at 610 and 658 nm. The QDs were selected so that their emission peaks match the absorbance bands of the dye. This overlap permits the absorption of the two forms of the chromoionophore to be indirectly monitored by the attenuation of the fluorescence of the dyes or the inner-filter effect of the chromoionophore.

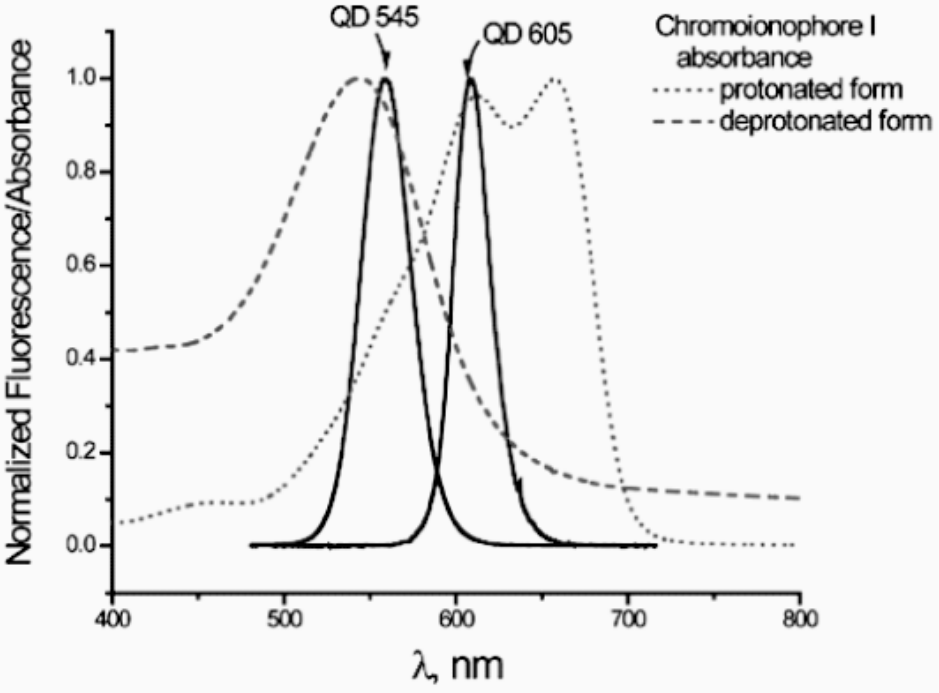

Figure 4.1. Spectral overlap of QDs emission and ETH 5294 absorbance. Protonated and deprotonated forms of the dye were measured in 10 mM HCl and 10 mM NaOH solutions, respectively. Each spectrum was normalized to its maximum intensity.

QDs with emission maxima at 545, 605 and 655 nm were utilized for sensor fabrication. The original solvent, decane, was replaced to minimize the number of solvents in the fabrication procedure. After several unsuccessful attempts to flocculate QDs (as suggested by Invitrogen), another procedure was applied. The QD solutions were kept in a desiccator under vacuum for 4 hr until complete solvent evaporation. The residues were then re-suspended in THF containing 3.5 M 1-DCT and were 5-fold more concentrated compared to original solutions. Replacement of decane with THF did not affect the position of QD's emission maxima and bandwidths (Figure 4.2). The 1-DCT was added to THF used for QD re-suspension to reduce the formation of QD aggregates, as described in literature[18, 23, 24].

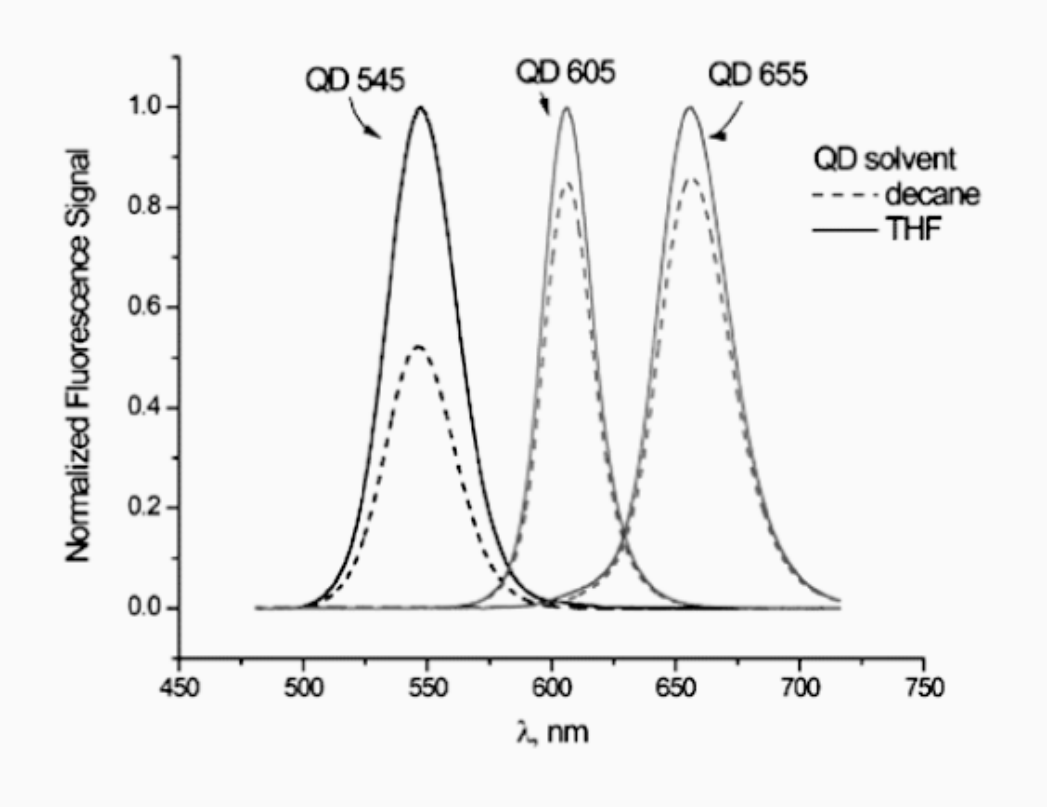

Figure 4.2. Emission of QD 545/605/655 suspensions in the original and replaced solvent, decane and THF, respectively. Spectra for each QD was normalized to the maximum fluorescence intensity in THF. The difference between spectra is caused by different degree of solvent evaporation between solvents.

The ratio of donor and acceptor – QDs and chromoionophore – was determined empirically to maximize optode's sensitivity. With higher concentrations of QD nanocrystals in the optode matrix, the change in QD emission was minor upon substantial change in the target ion activity. Significant reduction of the QD concentration resulted in an insufficient emission signal. An overlap of from fluorescence of ETH 5294 below 600 nm and QDs emission was observed. The final ratio of ETH5294:QD545:QD605 was $2 \cdot 10^3$:6:1. The final concentration of QD nanocrystals into polymeric matrix in these studies was significantly smaller comparing to previously reported studies.[20, 25]

To confirm a “soft” excitation conditions for the chromoionophore, QD655 and ETH 5294 were incorporated into a polymeric matrix to evaluate the membrane’s behavior when excited at different wavelengths. When the membrane was exposed to UV-light at 350 nm, a sole band at 655 nm was observed (Figure 4.3). In contrast, two emission bands, one from QD655 and one from the protonated form of ETH 5294 appeared when excited at 535 nm. No fluorescence is observed from ETH 5294 if the QDs doped ion optodes are excited with UV-light, which supports the assumption that the ETH 5294 is absorbing negligible UV radiation.

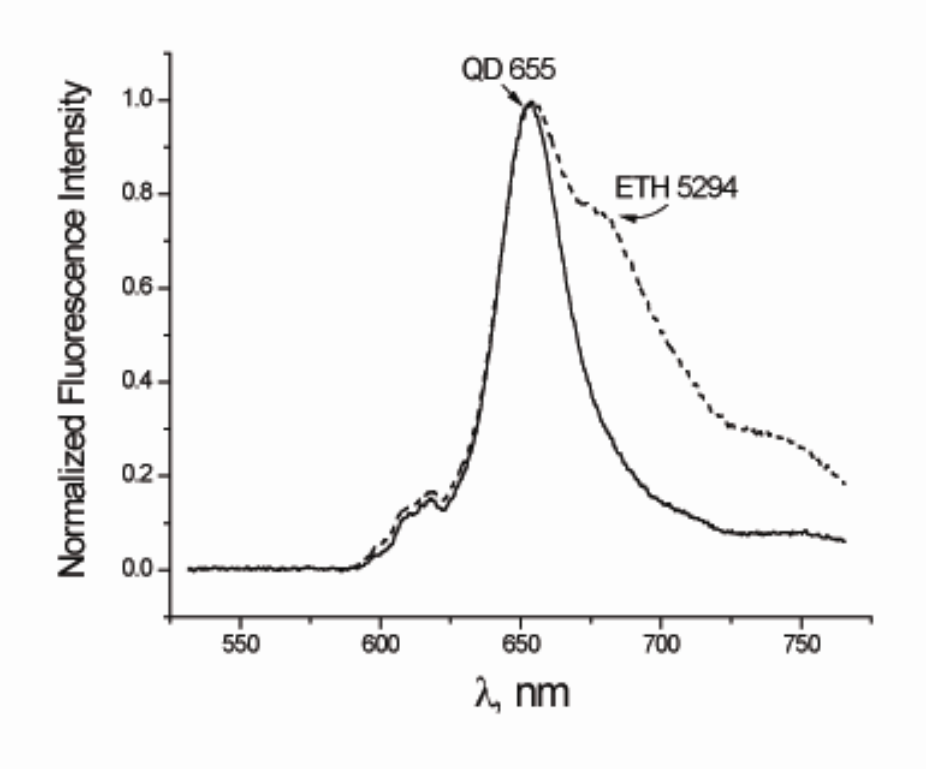

Figure 4.3. Fluorescence of a polymeric thin film containing ETH 5294 and QD655. The film was excited at 350 nm (solid line) and at 535 nm (dashed line).

To fabricate sensing beads, QDs in THF were added to the membrane cocktail and the polymeric mixture was rapidly injected into surfactant solution producing

polymeric spherical particles. An image of a typical batch of particles is shown in Figure 4.4 in both bright field and fluorescence modes. Fabricated particles appear to be smooth, spherical and uniform in size (~10 µm in diameter upon 1:2 dilution of the polymeric membrane with THF). The solvent displacement method allowed QD doped ion-optodes of controlled size to be produced in one step by addition of two extra components to a membrane cocktail. Complex organic syntheses for QDs ligand replacement or QD conjugation to a fluorophore were avoided leading to fast synthesis of ready-to-use particles. Their size is controlled based on the solvent nature and membrane concentration effects on the average size of particle fabricated via solvent displacement process.[21]

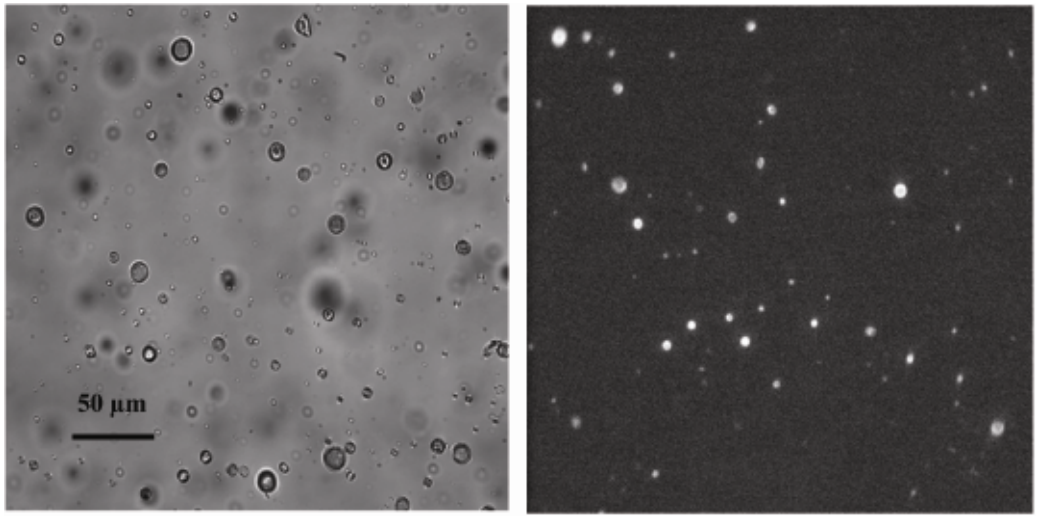

Figure 4.4. A bright field (left) and fluorescence (right) images of the QDs doped polymeric particles prepared via solvent displacement from the membrane cocktail diluted with 1:2 THF. The continuous phase contains 0.01% of Brij-35 (40x objective, excitation at 350 nm).

The proof-of-concept work was conducted on polymeric thin films. QDs exhibited a strong and stable emission signal when the films were conditioned at pH 7.0. Interestingly, the fluorescence decreased rapidly and permanently when

during studies at minimum and maximum protonation, in 10 mM NaOH and 10 mM HCl, respectively. This behavior suggests that QD nanocrystals are not stable at pH extremes.

The pH stability of the QDs was tested in QD suspensions, thin films and spherical particles. In Figure 4.5A, the QD suspension is observed to retain its bright color only under pH 8, also appearing pale yellow at pH 6. Incorporation of QDs into polymeric film (Figure 4.5B, dashed line) improved their stability, but an adequate working range was still limited to pH 6.5 – 8.5. Surprisingly, when the sample-solution pH-dependence of the polymeric spheres was probed, it was determined that the QDs were significantly more stable than those incorporated in films. The stability range expanded to pH 4 – 10 (Figure 4.5B, solid line). An extensive literature search revealed only a few papers that mentioned the pH instability of nanocrystals[26, 27], though the Invitrogen web-site states that Qdots are designed to work at neutral pH.

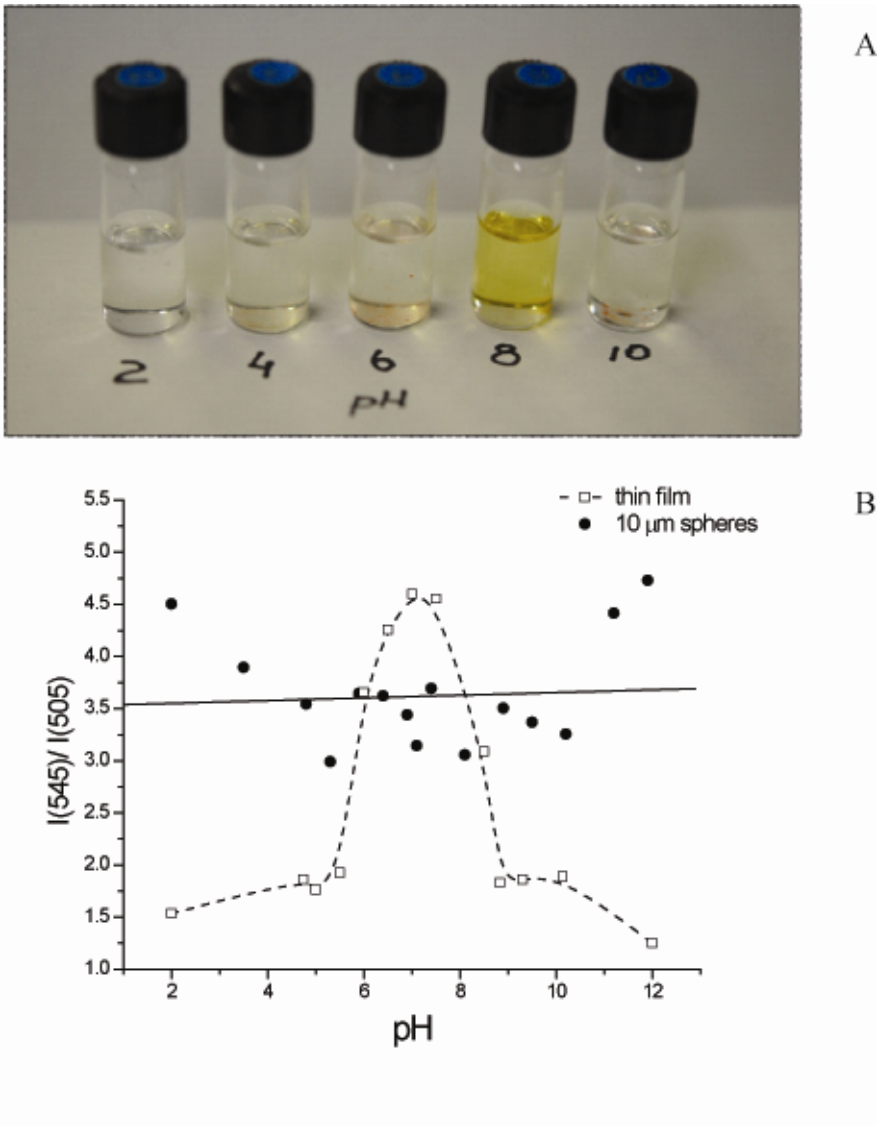

Figure 4.5. Stability of Invitrogen's ITK organic Qdots at different pH. QD suspensions (A), thin films and spherical beads (B) were studied. The Qdot suspension (A) was only stable around pH 8 – it preserved its bright yellow color. In all other cases, QDs collapse and lose their fluorescence irreversibly. The variation in signal from polymeric beads is attributed to variations in size of studied particles and probably different amounts of QDs in them. The data for spherical particles reveal a wider range of pH stability and were fitted with the linear least squares method (solid line).

We hypothesize that ion-optodes in the form of spherical particles are covered with surfactant molecules and have long hydrophobic “tails” which may additionally play a protective role along with the polymeric matrix. Thus, fabricated QD-doped spherical ion-optodes can be used in biological analysis because QD encapsulation reduces leaching of toxic compounds also protecting sensing components from an aggressive environment.

The quantum-dot doped sodium-selective sensor was fabricated with sodium ionophore X. Polymeric particles were obtained from the polymeric cocktail diluted 1:1 with THF. In all cases a single particle was selected for the each measurement and each calibration point is based on an average value from 5 different particles of approximately the same size (ca. 10 μm). The feasibility of using these small particle sensors was demonstrated. The typical fluorescence signals had a good *S/N* with an exposure time of 500 ms. (Figure 4.6).

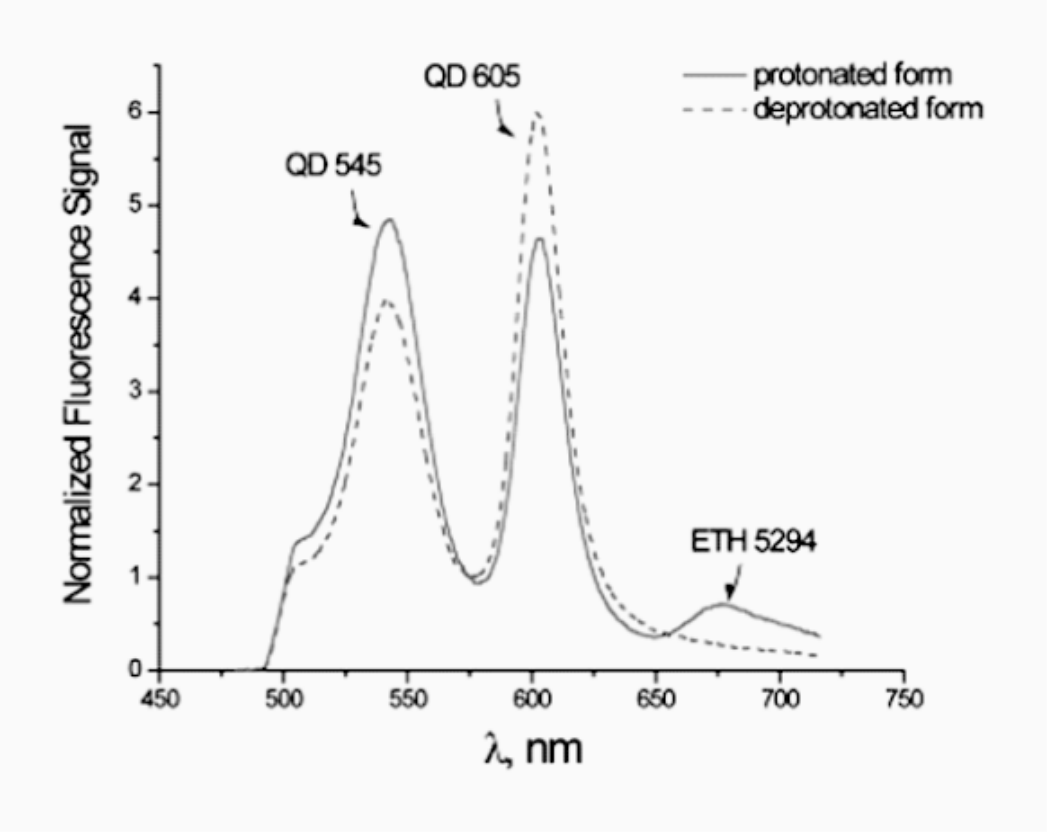

Figure 4.6. The fluorescence spectra of the fully protonated and fully deprotonated forms of a QD-doped ion optode. The protonated form was measured in a solution with pH 5.5. Minimum protonation was achieved in a solution containing 0.5 M Na^+ at pH 9.0. Measurements were taken from two independent particles and normalized to the emission intensity at 575 nm.

The calibration of sodium optodes at constant pH is shown in Figure 4.7. The degree of protonation (1-α) was calculated from the ratio of fluorescence signals of 545 nm relative to 605 nm. The dynamic range was found to be 0.1 mM to 0.1M at pH 7.5 and from pH 6.0 to pH 8.5 at 0.01 M Na^+. These results correlate with those obtained earlier for polymeric spherical optodes without QDs.[21]

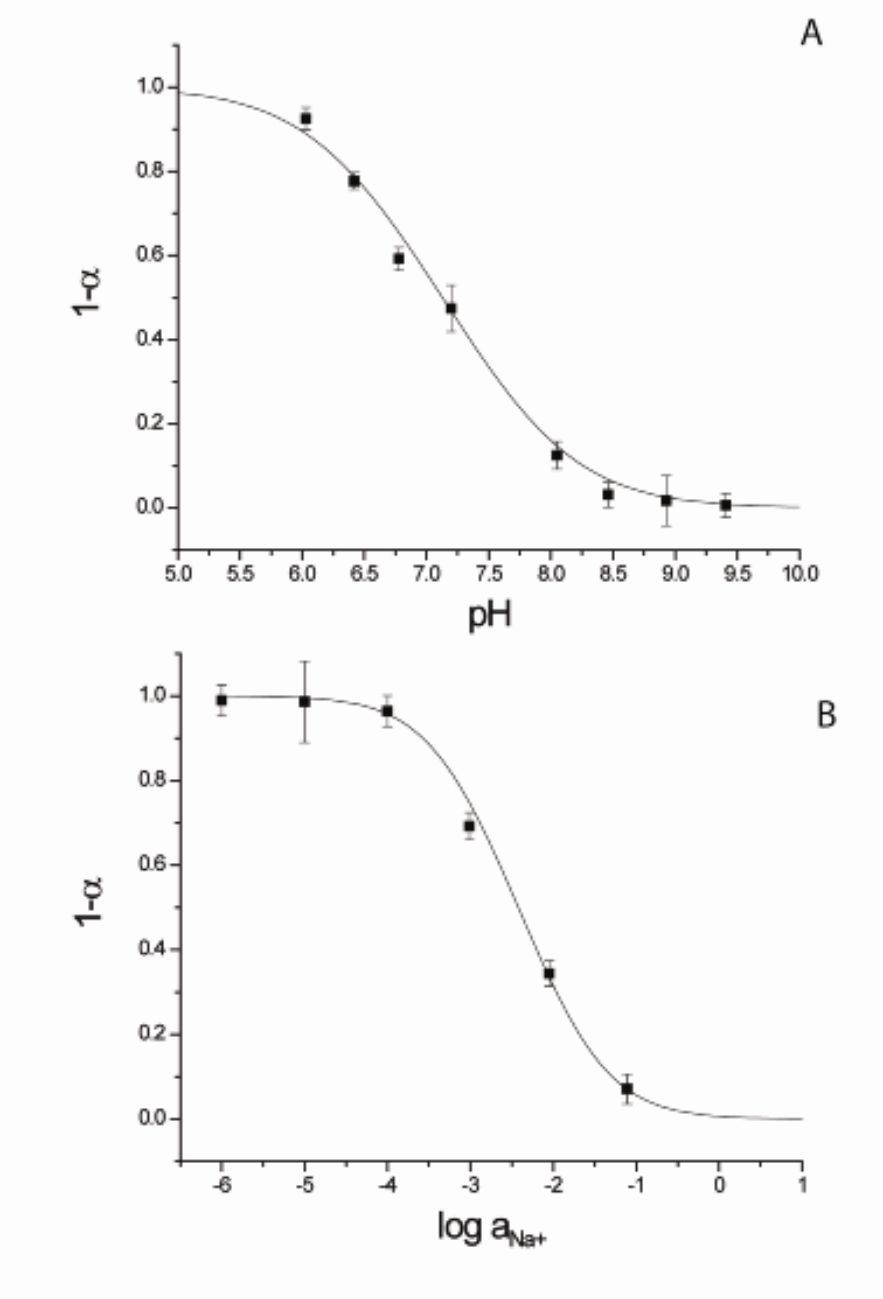

Figure 4.7. Responses of the sodium-selective optode for individual particles (10 ± 1 μm) with respect to A) pH at C(Na^+) = 10 mM; B) activity of Na^+ at pH 7.5, 10 mM TRIS buffer.

The experimental response was in an excellent agreement with the theoretical response[28]. The sensors demonstrated good reversibility and fast response time – the change in fluorescence was observed within seconds.

The ion-exchange constant observed for fabricated quantum-dot doped sensors was similar to that obtained experimentally in micron-sized PVC particles with the same sensing components, log K_{exch} = -5.4. This fact suggests that quantum dots used in this study are chemically inert and do not have any effect on sensor performance in contrast to previously reported results with home-synthesized quantum dots[20].

Support for this observation was provided by studying theζ-potential of the microparticle emulsion. As shown in Table 4.1, introduction of quantum dots or 1-DCT addition did not have a significant effect on the ζ-potential of 10-µm particles which remained at around -56 mV. In case of submicron-size particles, the ζ-potential increased to -40 mV upon introduction of CdSe nanocrystals indicating a positive net charge possessed by quantum dots. The change in ζ-potential with smaller particle size and higher of specific surface area, suggests that the quantum dots are located at the surface of a polymeric bead. These results indicate that caution is needed when working with nanosized ion optodes because their performance might be affected by this surface phenomenon.

Table 4.1. Zeta-potential measurements for the ion optodes of different composition.

Average particle size	PVC-DOS [a] spheres	Ion optodes	QDs doped ion optodes	QDs + 1-DCT doped optodes
10 µm	-59 ± 6 mV	-56 ± 8 mV	-53 ± 4 mV	-54 ± 7 mV
270 nm	-53 ± 7 mV	-55 ± 5 mV	-40 ± 3 mV	-45 ± 6 mV

[a] No sensing components. All samples were buffered at pH 7.

4.5. Conclusion

Semiconductor CdSe nanocrystals (QDs), due to their insensitivity to photobleaching, can function in ion-selective optodes as excitation donors in concert with organic dyes as acceptors. It was determined that QDs are extremely sensitive to hydrolysis in acidic and basic solutions. However, their encapsulation in surfactant coated polymeric spheres improves their stability over a wide pH range.

The fabrication of QD–doped, polymeric ion-optodes with the solvent displacement method proved to be a simple and reliable technique and allowed fine control of particle size. Introduction of commercial QDs directly into the polymeric membrane allows the absorption of photosensitive chromophores to be monitored without direct excitation with an intense light source. It was confirmed that QDs did not interfere with optode sensing components in microparticles. However, the surface charge of optodes becomes slightly less negative for submicron-sized particles. Further studies of the effect of CdSe QDs on the ion optode nanoprobes are needed, since net charge of QDs might interfere with overall sensor's response.

This method of QD-doped, optode fabrication could be implemented in a variety of sensing application with different sensing components and spectral ranges resulting from different particle size. The developed sensors can be potentially utilized in the measurements of physiological electrolytes in confined samples. Protection of QDs provided by a polymeric matrix makes them non-toxic probes suitable for introduction into living cells. Moreover, measurements over extended periods are possible due to high photostability of QDs emission signal.

4.6. Acknowledgement

This work was supported by the Office of Naval Research and the Oregon Nanoscience and Microtechnologies Institute.

4.7. References.

(1) Cui, R., Pan, H., Zhu, J., Chen, H. *Anal. Chem.* **2007**, *77*, 8494–8501.

(2) Fu, X., Kelong Huang, K., Liu, S. *Journal of Microbiological Methods* **2009**, *79*, 367-370.

(3) Lei, Y., Tang, H., Feng, M., Zou, B. *Journal of Nanoscience and Nanotechnology* **2009**, *9*, 5726–5730.

(4) So, M., Yao, H., Rao, J. *Biochemical and Biophysical Research Communications* **2008**, *374*, 419-423.

(5) Duconge, F., Pons, T., Pestourie, C., Herin, L., Theze, B., Gombert, K., Mahler, B., Hinnen, F., Kuehnast, B., Dolle, F., Dubertret, B., Tavitian, B. *Bioconjugate Chemistry* **2008**, *19*, 1921–1926.

(6) Mukthavaram, R., Wrasidlo, W., Hall, D., Kesari, S., Makale, M. *Bioconjugate Chemistry* **2011**, *22*, 1638–1644.

(7) Trapiella-Alfonso, L., Costa-Fernández, J.M., Pereiro, R., Sanz-Medel, A. *Biosensors and Bioelectronics* **2011**, *26*, 4753-4759

(8) Bruchez, M., Moronne, M., Gin, P., Weiss, S., Alivisatos, A. *Science* **1998**, *281*, 2013-2016.

(9) Jaiswal, J., Mattoussi, H., Mauro, J., Simon, S. *Nature Biotechnology* **2003**, *21*, 47-51.

(10) Resch-Genger, U., Grabolle, M., Cavaliere-Jaricot, S.,Nitschke, R.,Nann, T. *Nature Methods* **2008**, *5.9*, 763-775.

(11) Huang, C., Wu, C., Zhao, Y. *Journal of Nanoparticle Research* **2010**, *12*, 2153-2161.

(12) Clapp, A. R., Igor L. Medintz, I.L., Mattoussi, H. *ChemPhysChem* **2006**, *7*, 47–57.

(13) Robelek, R., Niu, L., Schmid, E. L., Knoll, W. *Anal. Chem.* **2004**, *76*, 6160-6165.

(14) Jin, W. J., Costa-Fernandez, J. M., Pereiro, R., Sanz-Medel, A. *Anal. Chim. Acta.* **2004**, *522*, 1-8.

(15) Wang, X., Boschetti, C., Ruedas-Rama, M., Tunnacliffe, A., Hall, E. *Analyst* **2010**, *135*, 1585-1591.

(16) Wang, Y., Mao, H., Wong, L. *Talanta* **2010**, *85*, 694-700.

(17) Tohda, K., Lu, H., Umezawa, Y., Gratzl, M. **2001**, *73*, 2070-2077.

(18) Dubach, J. M., Harjes, D., Clark, H. *J. Am. Chem. Soc.* **2007**, *129*, 8418-8419.

(19) Ruedas-Rama, M., Orte, A., Hall, E., Alvarez-Peza, J., Talaveraa, E. *Chem. Comm.* **2011**, *47*, 2898-2900.

(20) Xu, C., Bakker, E. *Anal. Chem.* **2007**, *79*, 3716-3723.

(21) Bychkova, V., Shvarev, A. *Anal. Chem.* **2009**, *81*, 2325–2331.

(22) Meier, P. C. *Anal. Chim. Acta.* **1982**, *136*, 363-368.

(23) Gattás-Asfura, K. M., Constantine, C.A., Lynn, M.J., Thimann, A.D., Ji X., Leblanc, R.M. *J. Am. Chem. Soc.* **2005**, *127*, 14640-14646.

(24) Walling, M. A., Novak, J. A., Shepard, J.R.E. *International Journal of Molecular Sciences* **2009**, *10*, 441-491.

(25) Ruedas-Rama, M. J., Wang, X., Hall, E. *Chem. Comm.* **2007**, 1544-1546.

(26) Aldana, J., Lavelle, N., Wang, Y., Peng, X. *J. Am. Chem. Soc.* **2005**, *127*, 2496-2504.

(27) Navarro, D. A. G., Watson, D.F., Aga, D.S., Banerjee, S. *Environmental Science & Technology* **2009**, *43*, 677-682.

(28) Bakker, E., Buhlmann, P., Pretsch, E. *Chem. Rev.* **1997**, *97*, 3083-3132.

CHAPTER 5

ENZYME LOGIC GATE ASSOCIATED WITH A SINGLE RESPONSIVE MICROPARTICLE: SCALING BIOCOMPUTING TO MICROSIZE SYSTEMS

Valeriya Bychkova, Alexey Shvarev*, Jian Zhou, Marcos Pita and Evgeny Katz*

Chemical Communications

Royal Society of Chemistry

Burlington House, Piccadilly, London W1J 0BA

Volume 46 (2010), 94-96

5.1. Abstract

A microsize biocomputing system based on enzyme logic processing of biochemical signals was developed. Optical transduction of pH signals generated in situ by the enzyme **OR** logic gate was achieved with the use of a single optode microparticle.

5.2. Introduction.

Unconventional chemical[1] and biochemical[2] computing systems meet several challenging problems: scaling up their complexity to mimic computing networks, scaling down their size to micro- and nanosystems and improving information processing for low noise performance. Different biomolecular tools, including proteins/enzymes[3], DNA[4], RNA[5], and whole cells[6] were used to assemble computing systems processing biochemical information. Recently emerged enzyme logic systems[7] have already achieved a complexity level to process several biochemical signals, mimicking logic network composed of 3–4 logic gates[8], while their optimization predicts low noise performance up to 10 concatenated gates[9]. Enzyme logic gates and their networks have been coupled with various signal-responsive materials, providing bulk material property changes in response to biochemical signals processed by the enzymes.[10] Logic operations performed at the nanoscale[11] or even at the single molecule level[12] have been reported for non-biochemical systems. The present communication is the first report on an enzyme logic system coupled with a single responsive microparticle aiming towards the miniaturization of biocomputing systems. Functional coupling of enzyme logic systems with signal-responsive materials has been realized via bulk[10] or local[13] pH changes generated by enzyme reactions in situ, resulting in the transition of switchable materials between two distinct states (e.g. shrunken and swollen polymers). It should be noted that pH-

controlled chemical transformations have also been used in various chemical logic systems without enzymes.[14] In the present work we used a single pH-sensitive microparticle to report on the pH changes generated by an enzyme logic system.

5.3. Experimental section.

Our **OR** logic gate system consisted of glucose oxidase (GOx, from *Aspergillus niger*, type X-S, E.C. 1.1.3.4; 3.1 unit mL^{-1}) and esterase (Est, from porcine liver, E.C. 3.1.1.1; 3.1 unit mL^{-1}) in a non-buffered 0.1 M Na_2SO_4 solution adjusted to an initial pH of 6.5 ± 0.3. The chemical inputs were 10 mM ethyl butyrate (input **A**) and 10 mM glucose (input **B**). Logic ‘‘**0**’’ and ‘‘**1**’’ in the input combinations refer to the absence and presence of the certain substance, respectively. The chemical input signals were applied to the system in four different combinations: **0**,**0**; **0**,**1**; **1**,**0** and **1**,**1**, where the first notation corresponds to signal **A** and the second to signal **B**. The enzyme system responded to the signals by oxidation of glucose biocatalyzed by GOx resulting in gluconic acid (note that O_2 was always present in the solution) and by hydrolysis of ethyl butyrate biocatalyzed by Est to yield butyric acid. Either (upon input signals **0**,**1**; **1**,**0**) or both (upon input signals **1**,**1**) produced acids resulted in the pH decrease finally reaching pH 4.6 ± 0.6. Only in the absence of both the input signals (**0**,**0**) did the system preserve its initial pH value, thus resembling the Boolean **OR** logic function. After the pH was decreased (inputs **0**,**1**; **1**,**0**; **1**,**1**), urease (from jack beans, E.C. 3.5.1.5; 10 unit mL^{-1}) was added to the solution, performing the **Reset** function activated by the addition of 4 mM urea, thus resulting in the biocatalytic formation of ammonia and increasing the pH to the initial level, Figure 5.1.

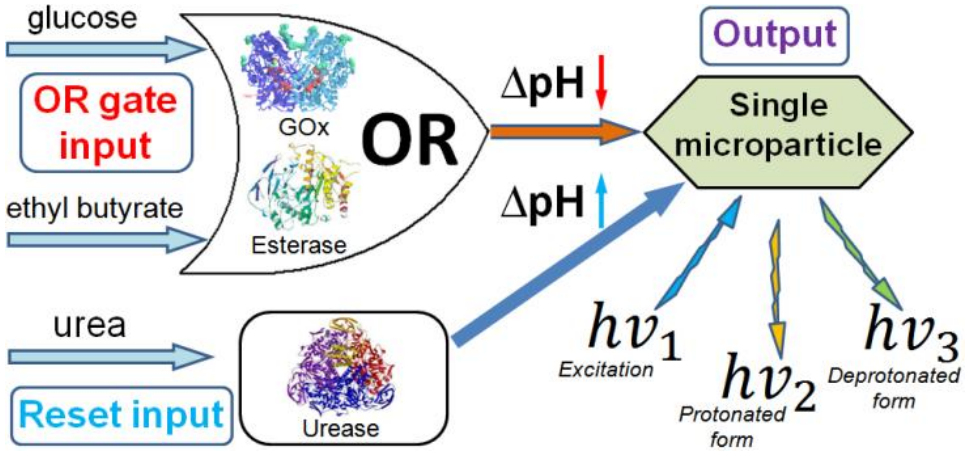

Figure 5.1. The **OR**–**Reset** enzyme system based on GOx–Est–Urease concerted operation producing in situ pH changes as the output signal when activated by glucose, ethyl butyrate and urea.

5.4. Results and discussion.

The pH changes generated in situ were detected by a single pH-responsive optode microparticle, 6.5 ± 0.5 μm in diameter. A typical ion-selective optode[15] contains an ionophore *L*, which selectively forms a complex with a primary metal ion I^{z+} (Na^+ in the present study) and a chromoionophore *Ind*, a lipophilic dye, that interacts with a reference ion (H^+ in the present study) and changes optical properties upon protonation. The third additive is a lipophilic cation-exchanger. Because the concentration of ion-exchanger in the matrix is limited, the competition between two ions (Na^+ and H^+) for the ion-exchange sites affects the fraction of protonated chromoionophore $IndH^+$ and determines the microsensor response. With the assumption that n_I is a stoichiometry of the ion-ionophore complex and z_I is the charge of the primary ion, the theoretical optode response function obeys eqn (5.1):[15]

$$a_I = (z_I K_{exch})^{-1} \left(\frac{\alpha}{1-\alpha} a_H\right)^{z_I} \left(\frac{R_T - (1-\alpha) Ind_T}{\left\{ L_T - (R_T - (1-\alpha) Ind_T) \left(\frac{n_I}{z_I}\right) \right\}^{n_I}} \right) \quad (5.1)$$

where K_{exch} is the ion-change constant. Subscript T denotes total concentrations of the ionophore (*L*), ion-exchanger (*R*), and chromoionophore (*Ind*), a_I and a_H are the activities of cation I^{z+} and hydrogen ion in the aqueous phase, respectively. The mole fraction of unprotonated chromoionophore is expressed as α. The mole fraction of the protonated form of the chromoionophore is related to the fluorescence signal according to eqn (5.2):

$$1 - \alpha = \frac{[IndH^+]}{Ind_T} = 1 - \frac{F_{max} - F}{F_{max} - F_{min}} \quad (5.2)$$

F is a measured fluorescence intensity ratio (at two wavelengths) measured in a given experiment, F_{min}, and F_{max} are the fluorescence intensity ratios at the minimum and maximum protonation of the chromoionophore, respectively, $[IndH^+]$ is the concentration of the protonated form, and Ind_T is a total concentration of the chromoionophore. The fluorescence intensity ratios at the minimum and maximum protonation were measured in 0.01 M solutions of NaOH and HCl, respectively.

The pH-reporting microparticle was immobilized on a glass support and the optical signals were read by an inverted fluorescence microscope (see details in the Appendices A and D). The fluorescence spectrum of the microparticle was determined by the ion exchange controlled by the pH value, Figure 5.2, thus allowing pH analysis in the solution adjacent to the microparticle. The chromoionophore protonated fraction (1 - α) was calculated from the fluorescence spectra, Figure 5.2, inset, using eqn (5.2). The microsensor stability, good reversibility and short response time allowed us to use a single optode microparticle for the continuous measurements and to control the localized rapid pH changes.[16]

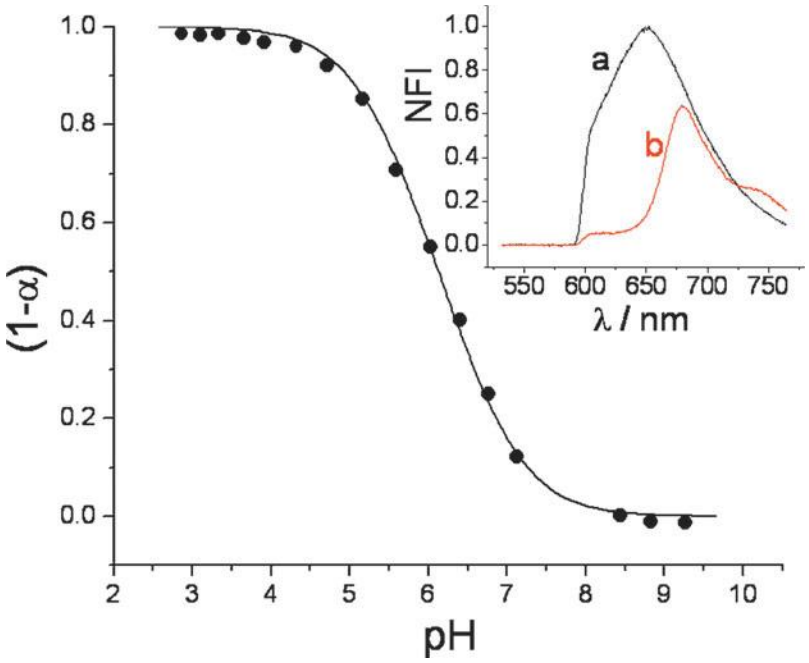

Figure 5.2. The protonated fraction of the chromoionophore in the optode microparticle as a function of the pH value. Inset: The fluorescence spectra of the fully unprotonated, 10 mM NaOH, (a) and fully protonated, 10 mM HCl, (b) chromoionophore: 9-(diethylamino)-5-octadecanoylimino-5H-benzo[a]phenox-azine. (NFI = normalized fluorescence intensity).

The pH evolutions generated in situ by the enzyme **OR** logic gate, Figure 5.3, followed by the **Reset** function were reported by a single microparticle in the form of fluorescence spectrum changes. A rough estimation, based on the amount of the pH-sensitive fluorescent dye in the microparticle (ca. 8.7×10^9 molecules), the concentration/activity of the enzymes and the time-period of the biocatalytic reactions, resulted in the conclusion that ca. 1×10^4 enzyme molecules localized in ca. 100–150 nm of the solution adjacent to the microparticle are able to produce the required pH changes. The diffusion layer thickness is relatively small compared to the sphere radius of the microparticle, meaning that the diffusion is fast (less than 10 ms) and the reaction occurs on the surface of the optode.

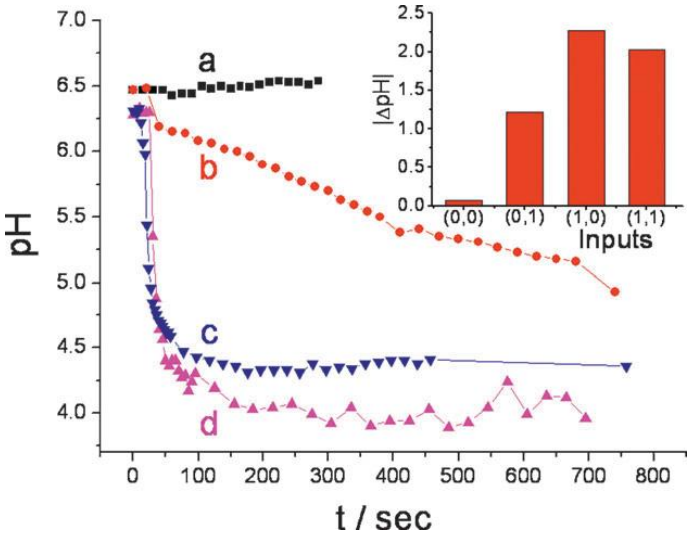

Figure 5.3. *In situ* pH changes generated by the enzyme **OR** logic gate and reported by the single optode microparticle upon application of the input signals: (a) **0**,**0**; (b) **0**,**1**; (c) **1**,**0** and (d) **1**,**1**, followed by the **Reset** function. Inset: Bar diagram featuring the pH changes generated by the different combinations of inputs.

In a control experiment, the enzyme-generated pH changes were produced in the absence of the chromoionophore functionalized microparticles. In this case no fluorescence was detected in the system.

It should be noted that in the present preliminary study the whole solution containing the reacting enzymes and their substrates produced the pH changes. However, only the adjacent thin-layer of the solution affected the fluorescent output signal generated by the microparticle. The obtained results provide the background for the next step, when the enzymes will be immobilized on the microparticle surface allowing not only their functional, but also spatial integration with the reporting microparticle. Also the complexity of the enzyme-signal processing system could be easily scaled up by applying multi-enzyme

systems converting many biochemical input signals to the pH changes and mimicking computing networks.[8b]

5.5. Conclusion.

The present work opens the way to enzyme logic networks associated with single responsive microparticles dramatically miniaturizing biocomputing systems. We anticipate that such miniaturized enzyme logic gates processing biochemical signals will find numerous analytical and biomedical applications, facilitate decision-making in connection to autonomous feedback-loop drug-delivery systems and will revolutionize monitoring and treatment of patients.

5.6. Acknowledgement.

NSF grants DMR-0706209, CCF-0726698, ONR grant N00014-08-1-1202 and SRC award 2008-RJ-1839G are gratefully acknowledged by the Clarkson University team. The authors from OSU acknowledge ONR and ONAMI for financial support (N00014-07-1-0457).

5.7. References.

1 (a) De Silva, A.P., Uchiyama, S. *Nat. Nanotechnol*., **2007**, *2*, 399–410; (b) Szacilowski, K. *Chem. Rev.*, **2008**, *108*, 3481–3548; (c) De Silva, A.P., Uchiyama, S., Vance, T.P., Wannalerse, B. *Coord. Chem. Rev*., **2007**, *251*, 1623–1632.

2 (a) Shao, X.G., Jiang, H.Y., Cai, W.S. *Huaxue Jinzha*n, **2002**, *14*, 37–46; (b) Fu, P. *Biotechnol. J.*, **2007**, *2*, 91–101; (c) Benenson, Y., Paz-Elizur, T., Adar, R., Keinan, E., Livneh, Z., Shapiro, E. *Nature*, **2001**, *414*, 430–434.

3 (a) Sivan, S., Lotan,N. *Biotechnol. Prog*., **1999**, *15*, 964–970; (b) Sivan, S., Tuchman, S., Lotan, N. *BioSystems*, **2003**, *70*, 21–33; (c) Deonarine, A.S., Clark, S.M., Konermann, L. *Future Gener. Comput. Syst.*, **2003**, *19*, 87–97; (d) Ashkenazi, G., Ripoll, D.R., Lotan, N., Scheraga, H.A. *Biosens. Bioelectron.*, **1997**, *12*, 85–95; (e) Unger, R., Moult, J. *Proteins: Struct., Funct., Bioinf.*, **2006**, *63*, 53–54.

4 (a) Stojanovic, M.N., Stefanovic, D., LaBean, T., Yan, H. in *Bioelectronics: From Theory to Applications, ed*. I. Willner, I., Katz, E. *Wiley-VCH, Weinheim*, **2005**, ch. *14*, pp. 427–455; (b) Saghatelian, A., Volcker, N.H., Guckian, K.M.,. Lin, V.S.Y., Ghadiri, M.R. *J. Am. Chem. Soc*., **2003**, *125*, 346–347; (c) Ashkenasy, G.,. Ghadiri, M.R. *J. Am. Chem. Soc*., **2004**, *126*, 11140–11141.

(5) Win, M.N., Smolke, C.D. *Science*, **2008**, *322*, 456–460.

(6) Simpson, M.L., Sayler, G.S., Fleming, J.T., Applegate, T. *Trends Biotechnol*., **2001**, *19*, 317–323.

(7) (a) Strack, G., Pita, M., Ornatska, M., Katz, E. *ChemBioChem*, 2008, *9*, 1260–1266; (b) Baron, R., Lioubashevski, O., Katz, E., Niazov, T., Willner, I. *J. Phys. Chem. A*, **2006**, *110*, 8548–8553.

(8) (a) Strack, G., Ornatska, M., Pita, M,. Katz, E. *J. Am. Chem. Soc*., **2008**, *130*, 4234–4235; (b) Privman, M., Tam, T.K., Pita, M., Katz, E. *J. Am. Chem. Soc*., **2009**, *131*, 1314–1321.

(9) (a) V. Privman, G. Strack, D. Solenov, M. Pita and E. Katz, *J. Phys. Chem. B*, 2008, *112*, 11777–11784; (b) V. Privman, M. A. Arugula, J. Hala´mek, M. Pita and E. Katz, *J. Phys. Chem. B*, **2009**, *113*, 5301–5310.

(10) (a) Tokarev, I., Gopishetty, V., Zhou, J., Pita, M., Motornov, M., Katz, E., Minko, S. *ACS Appl. Mater. Interfaces*, **2009**, *1*, 532–536; (b) Motornov, M., Zhou, J., Pita, M., Tokarev, I., Gopishetty, V., Katz, E., Minko, S. *Small*, **2009**,

5, 817–820; (c) Motornov, M., Zhou, J.,. Pita, M., Gopishetty, V., Tokarev, I., Katz, E., Minko, S. *Nano Lett*., **2008**, *8*, 2993–2997.

(11) (a) De Silva, A.P., Y. Leydet, Y., Lincheneau, C., McClenaghan, N.D. *J. Phys.: Condens. Matter*, **2006**, *18*, S1847–S1872; (b) Ogawa, A. Maeda, M. *Chem. Commun*., **2009**, 4666–4668.

(12) Stadler, R., Ami, S., Joachim C., Forshaw, M. *Nanotechnology*, **2004**, *15*, S115–S121.

(13) Pita, M., Tam,T.K., Minko, S., Katz, E. *ACS Appl. Mater. Interfaces*, **2009**, *1*, 1166–1168.

(14) Silvi, S., Constable, E.C., Housecroft, C.E., Beves, J.E., Dunphy, E.L., Tomasulo, M., Raymo, F.M., Credi, A. *Chem.–Eur. J.*, **2009**, *15*, 178–185.

(15) Bakker, E.; Buhlmann, P.; Pretsch, E. *Chem. Rev.* **1997**, *97*, 3083-3132.

(16) Bychkova, V.; Shvarev, A. *Anal. Chem.* **2009**, *81*, 2325-2331.

CHAPTER 6

CONCLUSION

The main objective of this work is to explore polymeric, ion-selective, optical sensors, so-called ion optodes, as analytical tools for biological measurements of physiological electrolytes. These carrier-based sensors represent a new class of nanoprobes capable of measuring changes in ion activity. They are based on the similar response mechanism as ISE's, and some of the same sensing compounds can be used. Optodes compared to ISE's also have a sensing chromoionophore. The optical properties (absorption or fluorescence) of the ion-optode change in response to the target ion activity in the sample solution

Ion optodes exhibit various advantages comparing to traditional ISE's or chromoionophore dyes in solution. All components are entrapped in a chemically inert matrix; hence, the toxicity of organic dyes and ionophores is minimized for measurements in living cells or their subcompartments. A polymeric optode sphere can be as small as 50 nm, which is only a small fraction of the cell volume. The analytical signal of such sensor depends on the equilibrium state of its bulk. Thus, the reduction of the optode volume provides much shorter response time and reduces the probe perturbation. These features, combined with the flexibility to easily change an optode's composition, make optodes an excellent tool for extra- and intracellular measurements of ionic fluxes.

In this dissertation, a novel and simple method for the fabrication of polymeric spherical sensing particles of controllable size is introduced. Solvent displacement is a simple single-batch process; all of the sensor's components can be dissolved in the disperse phase producing ready-to-use sensing particles. We successfully employed this technique to fabricate polymeric ion optodes with a PVC matrix plasticized by DOS.

The solvent displacement method provided consistent particle distributions with different solvents. Size distribution plots appeared unimodal and narrow. The low uniformity coefficient (0.4 – 0.6), in most cases, indicates monodisperse

distributions. The concentration and the nature of the surfactant had a little effect on the particle size distribution. The solvent composition provided a "coarse" control over the particle size distribution, while the concentration of a polymer in the membrane cocktail served as a "fine" tool. The size distribution was controllable in a continuous manner over the range of 200 nm-30 μm.

Ion optodes selective for sodium, potassium, and calcium cations were prepared with chromoionophore I, lipophilic ion-exchanger and sodium ionophore X, BME-44, and ETH 5234 for sodium, potassium, and calcium optodes, respectively. The sensors were fully functional with excellent selectivity to interfering ions. In addition to selectivity, the fabricated sensors demonstrated fast response time, high sensitivity and stability – over 6 weeks of a reproducible response.

The ability to control sensor size enabled evaluation of the dependence of the performance of ion optodes of the same chemical composition on size. The calibration curve shifted on the pH scale when comparing the response functions of micrometer and submicrometer sized particles for sodium, potassium and calcium probes. There is a strong correlation between the calculated specific surface area and the apparent ion-exchange constant for all three ion-optodes. The ion-exchange constant is directly proportional to the specific surface area for sodium and calcium optodes. However, the relationship between is reciprocal for potassium-selective sensors. No correlation between selectivity and the optode size was observed. We hypothesize that the observed effect is caused by surface phenomena contributing to the overall optode response. The results suggest that the response models, developed for the macroscopic ion optodes, cannot be easily applied to the probes at micron and sub-micron scale. Nevertheless, in the current literature the response equation is used assumed to be independent of size.

The main focus of the research in chapter 4 was to improve the stability of ion-selective optical sensors. Rapid photobleaching of the lipophilic dye precludes reliable measurements for longer-term monitoring of the sensor response. To overcome this shortcoming, quantum dots were incorporated into the polymeric matrix. QD nanocrystals, known for their unique optical properties, served as excitation donors for a lipophilic dye allowing "soft" excitation conditions for the latter. Two types of QDs with different emission wavelengths were simultaneously introduced into the sensing membrane allowing ratiometric measurements with a single light source. The solvent displacement method, as established earlier, provided fast and reliable fabrication with minimal modifications to fabricate QD-doped ion optodes. This novel procedure avoids additional time-consuming steps required in other methods, and produces ready-to-use sensing particles.

Incorporation of QDs into the sensor matrix improved their stability over a wider pH range and had little effect on ion optode response. Optodes were calibrated with respect to pH and sodium activity providing the same dynamic working range as optodes without QDs; calibration curves are in a good agreement with the theoretical prediction.

In chapter 5 one possible application of the fabricated polymeric optodes is discussed. A single reporting microparticle was used to simulate an enzyme-based Boolean logic gate. Miniaturization of chemical and biochemical computing systems must address several challenging problems: scaling up their complexity to mimic computing networks, scaling down size to micro- and nano-systems, and improving information processing for low-noise performance. The obtained results demonstrated proof of principle. The next step would involve immobilizing the enzymes on the microparticle surface, providing not only their functional, but also spatial integration with the reporting microparticle.

Although, optodes developed here are responsive for cations (Na^+, K^+, Ca^{2+}, H^+), introduction of an appropriate ionophore opens opportunities for detection of other physiologically and environmentally significant cations, anions and neutral molecules. With over 30 highly selective carriers available, the optodes could function in multicomponent sample matrixes with high selectivity to the target analyte.

The ion-selective optodes developed in this research are equilibrium sensors. Incorportion of photochemically activated compounds into the sensor matrix would provide enhanced sensor functionality, turning it into an active probe. In this mode controlled illumination causes a deviation from the ion-exchange equilibrium and induces non-equilibrium ion fluxes in the sensor-sample system. These optically controlled active probes can be used for the determination of the sample buffer capacity and photo-controlled titration at the micro- and nanoscale (see Appendix E).

Undoubtedly, ion optodes are generic and highly successful for chemical and biological imaging. Their further development and improvement is focused on measurement of new analytes in complex real-life samples.

BIBLIOGRAPHY

(1) Bakker, E., Buhlmann, P., Pretsch, E. *Chem. Rev.* **1997**, *97*, 3083-3132.

(2) Buhlmann, P., Pretsch, E., Bakker, E. *Chem. Rev.*, **1998**, *98*, 1593-1687.

(3) Maas, A.H.J., Siggaard-Andersen, O., Weisberg, H.F., Zijlstra, W.G. *Clinical Chemistry*, **1985**, *31(3)*, 482-485.

(4) Pethig, R., Menachery, A., Heart, E., Sanger, R.H., Smith, P.J.S. *IET Nanobiotechnology*, **2008**, *2(1)*, 28-35

(5) Hisamoto, H., Suzuki, K. *Trends in Anal. Chem.*, **1999**, *18(8)*, 513-524.

(6) Wygladacz, K., Bakker, E. *Anal. Chim. Acta.* **2005**, *532*, 61-69.

(7) Harris, D.C. *Quantitative Chemical Analysis*, 7th ed.; W. H. Freeman, **2006**.

(8) Diamond, D. *Principles of Chemical and Biological Sensors.* New York: Wiley, **1998**.

(9) Langmaier, J., Lindner, E. *Anal. Chim. Acta.* **2005**, *543*, 156-166.

(10) Frasco, M.F., Chaniotakis, N. *Sensors*, **2009**, *9*, 7266-7286.

(11) Smyder, J.A., Krauss, T.D. *Materials Today*, **2011**, *14(9)*, 382-387.

(12) Shiraki, T., Tsuchiya, Y., Shinkai, S. *Chemical Letter*, **2010**, *39*, 156-158.

(13) Tam, T.K., Zhou, J., Pita, M., Ornatska, M., Monko, S., Katz, E. *J. Am. Chem. Soc.*, **2008**, *130*, 10888-10889.

(14) Pita, M., Kramer, M., Zhou, J., Poghossian, A., Schoning, M.J., Fernandez, V.M., Katz, E. *ACS Nano*, **2008**, 2*(10)*, 2160–2166.

(15) Sun, X., Gao, J.P., Wang, Z.Y. *J. Am. Chem. Soc.*, **2008**, *130*, 8130-8131.

(16) Sze, A., Erickson. D., Ren, L., Li, D. *Journal of Colloidal and Interface Chemistry*, **2003**, *261*, 402-410.

(17) Shortreed, M., Bakker, E., Kopelman, R. *Anal. Chem.* **1996**, *68*, 2656-2662.

(18) Shortreed, M., Dourado, S., Kopelman, R. *Sensors Actuators B-Chemistry* **1997**, *38*, 8-12.

(19) Tan, W. H. S., Z.Y., Smith, S., Birnbaum, D., Kopelman, R. *Science* **1992**, *258*, 778-781.

(20) Ross, W. N. *Biophys. J.* **1993**, *64*, 1655-1656.

(21) Buck, S., Xu, H., Brasuel, M., Philbert, M.A., Kopelman, R. *Talanta* **2004**, *63*, 41-59.

(22) Morf, W. E., Seiler, K., Rusterholz, B., Simon, W. *Anal. Chem.* **1990**, *62*, 730-742.

(23) Ruedas-Rama, M. J., Wang, X., Hall, E, A.H. *Chem. Comm.* **2007**, 1544-1546.

(24) Goodey, A., Lavigne, J.J., Savoy, S.M., Rodriguez, M.D., Curey, T., Tsao, A., Simmons, G., Wright, J., Yoo, S., Sohn,Y., Anslyn, E.V., Shear, J.B., Neikirk, D. P., McDevitt, J.T. *J. Am. Chem. Soc.* **2001**, *123*.

(25) Xu, H., Aylott, J.W., Kopelman, R., Miller, T.J., Philbert, M.A. *Anal. Chem.* **2001**, *73*, 4124-4133.

(26) Clark, H. A., Barker, L.R., Kopelman, R., Hoyer, M., Philbert, M.A. *Sensors and Actuators B* **1998**, *51*, 12–16.

(27) Clark, H. A., Hoyer, M., Philbert, M.A., Kopelman, R. *Anal. Chem.* **1999**, *71*, 4831-4836.

(28) Clark, H. A. H., M., Parus, S., Philbert, M.A., Kopelman, R. *Mikrochimica Acta* **1999**, *131*, 121-128.

(29) Qin, Y., Peper, S., Bakker, E. *Electroanalysis* **2002**, *14*, 1375-1381.

(30) Peper, S., Ceresa, A., Qin, Y., Bakker, E. *Anal. Chim. Acta.* **2003**, *500*, 127-136.

(31) Seiler, K., Simon, W. *Anal. Chim. Acta.* **1992**, *266*, 73-87.

(32) Qin, Y., Bakker, E. *Talanta* **2002**, *58*, 909-918.

(33) Retter, R., Peper, S., Bell, M., Tsagkatakis, I., Bakker, E. *Anal. Chem.* **2002**, *74*, 5420-5425.

(34) Tsagkatakis, I., Peper, S., Retter, R., Bell, M., Bakker, E. *Anal. Chem.* **2001**, *73*, 6083-6087.

(35) Song, A., Parus, S., Kopelman, R. *Anal. Chem.* **1997**, *69*, 863-867.

(36) Dubach, J. M., Harjes, D.I., Clark, H.A. *Nano Lett.* **2007**, *7*, 1827-1831.

(37) Watts, A. S., Urbas, A.A., Moschou, E., Gavalas, V.G., Zoval, J.V., Madou, M., Bachas, L.G. *Anal. Chem.* **2007**, *79*, 8046-8054.

(38) Demuth, C., Spichiger, U.E. *Anal. Chim. Acta.* **1997**, *355*, 259-268.

(39) Wygladacz, K., Bakker, E. *The Analyst* **2006**, *132*, 268-272.

(40) Xu, C., Qin, Y., Bakker, E. *Talanta* **2004**, *63*, 180-184.

(41) Koo, Y. L., Cao, Y., Kopelman, R., Koo,S.M., Brasuel, M., Philbert, M.A. *Anal. Chem.* **2004**, *76*, 2498-2505.

(42) Brasuel, M., Kopelman, R., Miller, T.J., Tjakens, R., Philbert, M.A. *Anal. Chem.* **2001**, *73*, 2221-2228.

(43) Lerchi, M., Reitter, E., Simon, W., Pretsch, E., Chowdhurry, D.A., Kamata, S. *Anal. Chem.* **1994**, *66*, 1713-1717.

(44) Shamsipur, M., Rouhani, S., Mohajeri, A., Ganjali, M.R. *Anal. Bioanal. Chem.* **2003**, *375*, 692-697.

(45) Wygladacz, K., Radu, A., Xu, C., Qin, Y., Bakker, E. *Anal. Chem.* **2005**, *77*, 4706-4712.

(46) Méallet-Renault, R., Hérault, A., Vachon, J., Pansu, R.B., Amigoni-Gerbier, S., Larpent, C. *Photochem. Photobiol. Sci.* **2006**, *5*, 300-310.

(47) Anticó, E., Lerchi,M., Rusterholz, B., Achermann, N., Badertscher, M., Valiente, M., Pretsch, E. *Anal. Chim. Acta.* **1999**, *388*, 327-338.

(48) Kellar, K. L.; Iannone, M. A. *Experimental Hematology* **2002**, *30*, 1227-1237.

(49) Vignali, D. A. A. *Journal of Immunological Methods* **2000**, *243*, 243-255.

(50) Dickinson, T. A.; Michael, K. L.; Kauer, J. S.; Walt, D. R. *Anal. Chem.* **1999**, *71*, 2192-2198.

(51) Fulton, R. J.; McDade, R. L.; Smith, P. L.; Kienker, L. J.; Kettman, J. R. J. *Clin.Chem.* **1997**, *43*, 1749-1756.

(52) Oleschuk, R. D.; Shultz-Lockyear, L. L.; Ning, Y.; Harrison, D. J. *Anal. Chem.* **2000**, *72*, 585-590.

(53) Buck, S. M.; Koo, Y. E. L.; Park, E.; Xu, H.; Philbert, M. A.; Brasuel, M. A.; Kopelman, R. *Current Opinion In Chemical Biology* **2004**, *8*, 540-546.

(54) Telting-Diaz, M.; Bakker, E. *Anal. Chem.* **2002**, *74*, 5251-5256.

(55) Tseng, C. M.; Lu, Y. Y.; El-Aasser, M. S.; Vanderhoff, J. W. *Journal of Polymer Science Part A: Polymer Chemistry* **1986**, *24*, 2995-3007..

(56) Peper, S.; Tsagkatakis, I.; Bakker, E. *Anal. Chim. Acta.* **2001**, *442*, 25-33.

(57) Chu, B. S.; Ichikawa, S.; Kanafusa, S.; Nakajima, M. *J. Agric. Food Chem.* **2007**, *55*, 6754-6760.

(58) Reis, C. P.; Neufeld, R. J.; Ribeiro, A. J.; Veiga, F. *Nanomed.* **2006**, *2*, 8-21.

(59) Ribeiro, H. S.; Chu, B.-S.; Ichikawa, S.; Nakajima, M. *Food Hydrocolloids* **2008**, *22*, 12-17.

(60) Meier, P. C. *Anal. Chim. Acta* **1982**, *136*, 363.

(61) Dubach, J. M.; Harjes, D. I.; Clark, H. A. *J. of the Am. Chem. Soc.* **2007**, *129*, 8418-8419.

(62) Kurihara, K.; Ohtsu, M.; Yoshida, T.; Abe, T.; Hisamoto, H.; Suzuki, K. *Anal. Chem.* **1999**, *71*, 3558-3566.

(63) Bychkova, V.; Shvarev, A. *Anal. Chem.* **2009**, *81*, 2325-2331.

(64) Naujok, R. R.; Paul, H. J.; Corn, R. M. *J. Phys. Chem.* **1996**, *100*, 10497-10507.

(65) Tamburello-Luca, A. A.; Hebert, P.; Antoine, R.; Brevet, P. F.; Girault, H. H. *Langmuir* **1997**, *13*, 4428-4434.

(66) Zhao, X.; Subrahmanyan, S.; Eisenthal, K. B. *Chem. Phys. Lett.* **1990**, *171*, 558-562.

(67) Cui, R., Pan, H., Zhu, J., Chen, H. *Anal. Chem.* **2007**, *77*, 8494–8501.

(68) Fu, X., Kelong Huang, K., Liu, S. *Journal of Microbiological Methods* **2009**, *79*, 367-370.

(69) Lei, Y., Tang, H., Feng, M., Zou, B. *Journal of Nanoscience and Nanotechnology* **2009**, *9*, 5726–5730.

(70) So, M., Yao, H., Rao, J. *Biochemical and Biophysical Research Communications* **2008**, *374*, 419-423.

(71) Duconge, F., Pons, T., Pestourie, C., Herin, L., Theze, B., Gombert, K., Mahler, B., Hinnen, F., Kuehnast, B., Dolle, F., Dubertret, B., Tavitian, B. *Bioconjugate Chemistry* **2008**, *19*, 1921–1926.

(72) Mukthavaram, R., Wrasidlo, W.,Hall, D., Kesari, S., Makale, M. *Bioconjugate Chemistry* **2011**, *22*, 1638–1644.

(73) Trapiella-Alfonso, L., Costa-Fernández, J.M., Pereiro, R., Sanz-Medel, A. *Biosensors and Bioelectronics* **2011**, *26*, 4753-4759

(74) Bruchez, M., Moronne,M., Gin, P., Weiss, S., Alivisatos, A. *Science* **1998**, *281*, 2013-2016.

(75) Jaiswal, J., Mattoussi, H., Mauro, J., Simon, S. *Nature Biotechnology* **2003**, *21*, 47-51.

(76) Resch-Genger, U., Grabolle, M.,Cavaliere-Jaricot, S.,Nitschke, R.,Nann, T. *Nature Methods* **2008**, *5.9*, 763-775.

(77) Huang, C., Wu, C., Zhao, Y. *Journal of Nanoparticle Research* **2010**, *12*, 2153-2161.

(78) Clapp, A. R., Igor L. Medintz, I.L., Mattoussi, H. *Chem Phys Chem* **2006**, *7*, 47–57.

(79) Robelek, R., Niu, L., Schmid, E. L., Knoll, W. *Anal. Chem.* **2004**, *76*, 6160-6165.

(80) Jin, W. J., Costa-Fernandez, J. M., Pereiro, R., Sanz-Medel, A. *Anal. Chim. Acta.* **2004**, *522*, 1-8.

(81) Wang, X., Boschetti, C., Ruedas-Rama, M., Tunnacliffe, A., Hall, E. *Analyst* **2010**, *135*, 1585-1591.

(82) Wang, Y., Mao, H., Wong, L. *Talanta* **2010**, *85*, 694-700.

(83) Tohda, K., Lu, H., Umezawa, Y., Gratzl, M. **2001**, *73*, 2070-2077.

(84) Ruedas-Rama, M., Orte, A., Hall, E., Alvarez-Peza, J., Talaveraa, E. *Chem. Comm.* **2011**, *47*, 2898-2900.

(85) Xu, C., Bakker, E. *Anal. Chem.* **2007**, *79*, 3716-3723.

(86) Gattás-Asfura, K. M., Constantine, C.A., Lynn, M.J., Thimann, A.D., Ji X., Leblanc, R.M. *J. Am. Chem. Soc.* **2005**, *127*, 14640-14646.

(87) Walling, M. A., Novak, J. A., Shepard, J.R.E. *International Journal of Molecular Sciences* **2009**, *10*, 441-491.

(88) Aldana, J., Lavelle, N., Wang, Y., Peng, X. *J. Am. Chem. Soc.* **2005**, *127*, 2496-2504.

(89) Navarro, D. A. G., Watson, D.F., Aga, D.S., Banerjee, S. *Environmental Science & Technology* **2009**, *43*, 677-682.

(90) De Silva, A.P., Uchiyama, S. *Nat. Nanotechnol*., **2007**, *2*, 399–410.

(91) Szacilowski, K. *Chem. Rev.*, **2008**, *108*, 3481–3548.

(92) De Silva, A.P., Uchiyama, S., Vance, T.P., Wannalerse, B. *Coord. Chem. Rev*., **2007**, *251*, 1623–1632.

(93) Shao, X.G., Jiang, H.Y., Cai, W.S. *Huaxue Jinzha*n, **2002**, *14*, 37–46.

(94) Fu, P. *Biotechnol. J*., **2007**, *2*, 91–101.

(95) Benenson, Y., Paz-Elizur, T., Adar, R., Keinan, E., Livneh, Z., Shapiro, E. *Nature*, **2001**, *414*, 430–434.

(96) Sivan, S., Lotan,N. *Biotechnol. Prog*., **1999**, *15*, 964–970.

(97) Sivan, S., Tuchman, S., Lotan, N. *BioSystems*, **2003**, *70*, 21–33.

(98) Deonarine, A.S., Clark, S.M., Konermann, L. *Future Gener. Comput. Syst.*, **2003**, *19*, 87–97.

(99) Ashkenazi, G., Ripoll, D.R., Lotan, N., Scheraga, H.A. *Biosens. Bioelectron.*, **1997**, *12*, 85–95.

(100) Unger, R., Moult, J. *Proteins: Struct., Funct., Bioinf.*, **2006**, *63*, 53–54.

(101) Stojanovic, M.N., Stefanovic, D., LaBean, T., Yan, H. in *Bioelectronics: From Theory to Applications, ed*. I. Willner, I., Katz, E. *Wiley-VCH, Weinheim*, **2005**, ch. *14*, pp. 427–455.

(102) Saghatelian, A., Volcker, N.H., Guckian, K.M.,. Lin, V.S.Y., Ghadiri, M.R. *J. Am. Chem. Soc.*, **2003**, *125*, 346–347.

(103) Ashkenasy, G.,. Ghadiri, M.R. *J. Am. Chem. Soc.*, **2004**, *126*, 11140–11141.

(104) Win, M.N., Smolke, C.D. *Science*, **2008**, *322*, 456–460.

(105) Simpson, M.L., Sayler, G.S., Fleming, J.T., Applegate, T. *Trends Biotechnol*., **2001**, *19*, 317–323.

(106) Strack, G., Pita, M., Ornatska, M., Katz, E. *Chem Bio Chem*, **2008**, *9*, 1260–1266.

(107) Baron, R., Lioubashevski, O., Katz, E., Niazov, T., Willner, I. *J. Phys. Chem. A*, **2006**, *110*, 8548–8553.

(108) Strack, G., Ornatska, M., Pita, M,. Katz, E. *J. Am. Chem. Soc*., **2008**, *130*, 4234–4235.

(109) Privman, M., Tam, T.K., Pita, M., Katz, E. *J. Am. Chem. Soc*., **2009**, *131*, 1314–1321.

(110) Privman, V. Strack, G., Solenov, D., Pita, M., Katz, E. *J. Phys. Chem. B*, 2008, *112*, 11777–11784.

(111) Privman, V., Arugula, M.A., Hala´mek, J., Pita, M., Katz, E. *J. Phys. Chem. B*, **2009**, *113*, 5301–5310.

(112) Tokarev, I., Gopishetty, V., Zhou, J., Pita, M., Motornov, M., Katz, E., Minko, S. *ACS Appl. Mater. Interfaces*, **2009**, *1*, 532–536.

(113) Motornov, M., Zhou, J., Pita, M., Tokarev, I., Gopishetty, V., Katz, E., Minko, S. *Small*, **2009**, *5*, 817–820.

(114) Motornov, M., Zhou, J., Pita, M., Gopishetty, V., Tokarev, I., Katz, E., Minko, S. *Nano Lett*., **2008**, *8*, 2993–2997.

(115) De Silva, A.P., Y. Leydet, Y., Lincheneau, C., McClenaghan, N.D. *J. Phys.: Condens. Matter*, **2006**, *18*, S1847–S1872.

(116) Ogawa, A. Maeda, M. *Chem. Commun*., **2009**, 4666–4668.

(117) Stadler, R., Ami, S., Joachim C., Forshaw, M. *Nanotechnology*, **2004**, *15*, S115–S121.

(118) Pita, M., Tam, T.K., Minko, S., Katz, E. *ACS Appl. Mater. Interfaces*, **2009**, *1*, 1166–1168.

(119) Silvi, S., Constable, E.C., Housecroft, C.E., Beves, J.E., Dunphy, E.L., Tomasulo, M., Raymo, F.M., Credi, A. *Chem.–Eur. J*., **2009**, *15*, 178–185.

(120) Shvarev, A. *J. Am. Chem. Soc.*, **2006**, *128*, 7138-7139.

APPENDICES

APPENDIX A

GENERAL INFORMATION ON SYNTHESIS AND RESPONSE MECHANISM OF ION OPTODES

A.1. Fabrication of the optode beads.

A solvent displacement method described recently was used to produce the optodes. [1] A small (~ 8 mL) vial was filled with an aqueous solution of a surfactant (0.01% wt. Brij-35). The surfactant solution was stirred using a small magnetic stir bar at approximately 100 rpm. A small amount (100-400 μL depending on the dilution ratio) of the polymer solution was drawn into a disposable syringe. The syringe was held above the vial, the needle was positioned 4-5 mm above the solution surface, and the polymeric solution was rapidly injected. Instantaneous precipitation produced a stable milky suspension which often contained a small fraction of coagulum.

A.2. Instrumentation.

A custom-made flow cell (similar to the VacuCel™ produced by C&L Instruments, Hershey, PA) was used. A microscope cover glass was held in place by a vacuum between two o-rings forming a transparent wall of a flow cell. The cell was connected to a peristaltic pump (Variable-Flow MiniPump, Fisher Scientific, Pittsburgh, PA) operating at 0.1 mL/s. The measurements were carried out in a "stop-flow" mode. The pH was measured using a pH-meter (Accumet XL-15, Fisher Scientific, Pittsburgh, PA) with a double-junction combination glass pH-electrode.

The optical setup included an inverted fluorescence microscope (Olympus IX-71, Olympus, Center Valley, PA) with an attached microspectrometer (Acton Microspec MS-2150) and a PIXIS-512 cooled CCD camera (both from Princeton Instruments, Trenton, NJ). The microspectrometer allows for switching between direct imaging (nondispersed) and spectral imaging (dispersed) modes. A mirror and a diffraction grating are attached to the motorized computer-controlled turret

providing fast switching capability; thus, the same camera can be used for both direct and spectral imaging (Figure A.1).

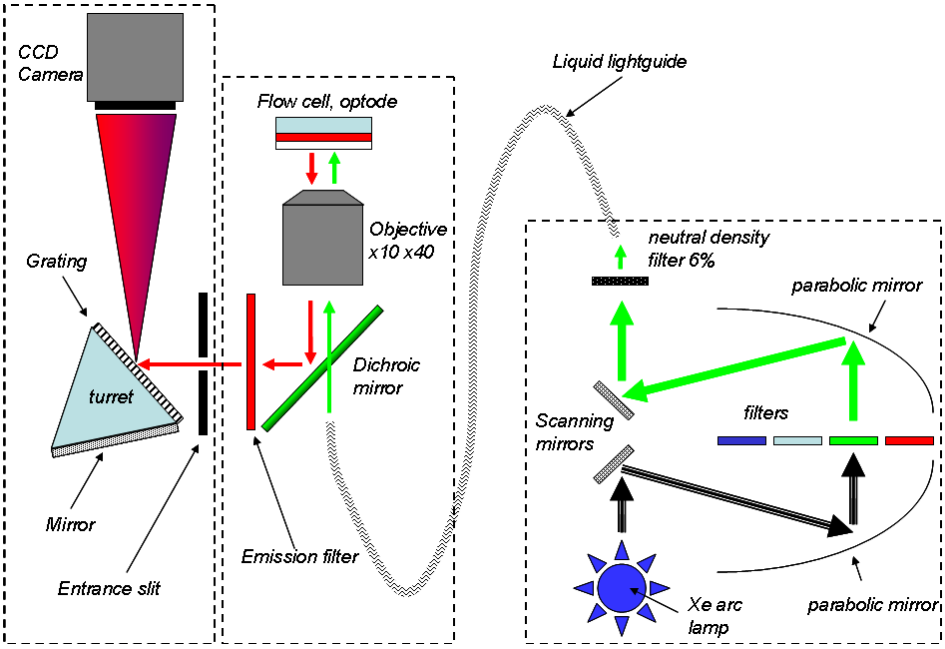

Figure A.1. The schematic diagram of the experimental setup: light source, fluorescence microscope, spectrometer.

A fast wavelength switch DG-4 (Sutter Instrument, Novato, CA) with a 300-W xenon arc lamp and a 535 (±25) nm filter was used a light source. A filter cube consisted of a 565 nm dichroic mirror and a 600-nm long-pass emission filter. The long-pass filter in the fluorescence cube allowed us to record the spectra within the 600-800 nm region. The microscope was equipped with 40x/0.17 objective (UPlanSApo, Olympus, Center Valley, PA).

The camera and the spectrometer were controlled by a PC running WinSpec32 software (Princeton Instruments, Trenton, NJ) in the slave mode. A custom-programmed microcontroller was used to control the DG-4 and generate triggering signals for the CCD camera. Detection was performed with a 220-ms

pulse of excitation light (550 nm) with simultaneous triggering of the camera shutter for a 200-ms exposure.

At first, the microspectrometer was switched to the direct imaging mode, which allowed examining a sample and selecting a particle of interest. This preliminary selection of the particle was done to avoid photobleaching. Then the microscope stage was moved in order to position the particle in the center of the field of view and the slit was placed at the spectrometer entrance. The setup was switched to the fluorescence mode, and a fluorescence spectrum was acquired.

The microscope table was controlled by a combination of a motorized stage (H107, Prior Scientific, Rockland, MA) and a piezoelectric stage (P517-K024, Physik Instrumente, Irvine, CA) built in-house. The mechanical positioner allowed a coarse displacement within ± 20 mm with a ± 1-μm resolution. The piezoelectric stage had a 100 μm throw with a 1 nm closed-loop resolution. In practice, the latter was limited to ± 25 nm due to the resolution of the 12-bit DAC (USB-6009, National Instruments, Austin, TX) used to control the analog piezoelectric stage controller.

The fluorescence of the chromoionophore was measured at 650 and 680 nm which corresponded to the fluorescence maxima of the deprotonated and protonated forms of the dye.

A.3. The optode response measurements.

A typical cation-selective optode[1] contains an ionophore *L*, which selectively forms a complex with a primary (metal) ion I^{z+}, and a chromoionophore *Ind*, a lipophilic dye that interacts with a reference ion (usually, hydrogen) and undergoes changes in optical properties upon protonation. The third additive is a lipophilic cation-exchanger. Since the concentration of ion-exchanger in the

matrix is limited, the competition between two ions for the ion-exchange sites affects the fraction of protonated chromoionophore $IndH^+$ and determines the sensor response. If the pH in the aqueous sample is fixed (buffered), the optode responds to the metal activity in the sample or vice versa. With the assumption that n_I is the stoichiometry of the ion-ionophore complex with the respect to I^{z+} and z_I is the charge of the primary ion, the theoretical optode response function obeys the following equation [1]:

$$a_I = (z_I K_{exch})^{-1} \left(\frac{\alpha}{1-\alpha} a_H\right)^{z_I} \left(\frac{R_T - (1-\alpha)Ind_T}{\left\{L_T - (R_T - (1-\alpha)Ind_T)\left(\frac{n_I}{z_I}\right)\right\}^{n_I}}\right) \quad \text{(A.1)}$$

where K_{exch} is the ion-exchange constant. The subscript T denotes the total concentrations of the ionophore (L), the ion-exchanger (R), or the chromoionophore (Ind). The symbols a_I and a_H represent the activities of the cation I^{z+} and hydrogen in the aqueous phase, respectively. The mole fraction of unprotonated chromoionophore is expressed as α. The mole fraction of the protonated form of the chromoionophore is related to the fluorescence signal as:

$$1 - \alpha = \frac{[IndH^+]}{Ind_T} = 1 - \frac{F_{max} - F}{F_{max} - F_{min}} \quad \text{(A.2)}$$

where F is the measured fluorescence intensity ratio (at two wavelengths for the protonated and unprotonated forms) measured in a given experiment, F_{min}, and F_{max} are the fluorescence intensity ratios at the minimum and maximum protonation of the chromoionophore, respectively, [$IndH^+$] is the concentration of the protonated form, and Ind_T is a total concentration of the chromoionophore. The intensity ratios at the minimum and maximum protonation were measured in 0.01 M solutions of NaOH and HCl, respectively.

The pH of the solutions was maintained with 10 mM of TRIS or with 10 mM MOPS buffers and a universal buffer solution containing 3.3 mM citric acid, 5.5 mM boric acid and 5.0 mM phosphoric acid adjusted to the desired pH value

with 1 M KOH. All experiments were conducted at ambient temperature (23 ± 2 °C). Activity coefficients were calculated according to Debye-Hückel formalism. [2]

A.4. References.

(1) Bakker, E.; Buhlmann, P.; Pretsch, E. *Chem. Rev.* **1997**, *97*, 3083-3132.

(2) Meier, P. C. *Anal. Chim. Acta* **1982**, 136, 363.

APPENDIX B

EXPERIMENTAL DETAILS ON ION OPTODE FABRICATION AND CHARACTERIZATION

B.1. Polymeric beads fabrication.

The monodispersity of the size distribution was further improved by vacuum filtration. Filters with differing pore sizes were used for emulsions created by diluting the dissolved cocktail solution with varying amounts of THF. Specifically, a Whatman no. 1 filter (pore size 11 μm) was used for the 1:1 dilution, a Whatman no. 3 cellulose filter (pore size 6.0 μm) was used for the 1:5 dilution, a glass microfiber filter GF/D (pore size 2.7 μm) was used for the 1:7 dilution, a glass microfiber filter GF/B (pore size 1.0 μm) was used for the 1:8 dilution, and a Whatman no. NL17 polyamide membrane (pore size 0.45 μm) was used to filter the 1:10 dilution.

B.2. Particle size distribution.

We performed the size characterization using the low-angle laser light scattering (LALLS) method in order to characterize the size distribution within the 50 nm-50 μm range. All of the measurements were carried out using a Hydro 2000S-AWA 2001 particle size analyzer and Mastersizing 2000 software (Malvern Inst., Westborough, MS). All solutions contained a small fraction of surfactant (0.001% - 0.01% wt.). Ionic strength and pH were not controlled.

APPENDIX C

EXPERIMENTAL DETAILS ON ZETA-POTENTIAL MEASUREMENTS AND RESPONSE CALCULATIONS OF QUANTUM DOTS DOPED ION OPTODES

C.1. Zeta-potential measurements.

Emulsions with 2 different size distributions were compared. Polymer solution was diluted with THF in 1:2 and 1:8 ratios to obtain emulsions with average particle size 10 μm and 0.27 μm [1]. The monodispersity of the size distribution was further improved by vacuum filtration. Specifically, a Whatman no. 1 filter (pore size 11 μm) was used for the 1:2 dilution, a glass microfiber filter GF/B (pore size 1.0 μm) was used for the 1:8 dilution. All samples contained 0.003M NaCl at pH 7.0.

C.2. Response measurements.

Detection was performed with a 500-ms pulse of excitation light (350 or 535 nm) with simultaneous triggering of the camera shutter for a 500-ms exposure.

The fluorescence of quantum dots was measured at 545 and 605 nm which corresponded to the fluorescence maxima of the deprotonated and protonated forms of the dye.

The intensity ratios at the maximum and minimum protonation were measured in a solution with pH 5.5 and a solution with pH 9.0 containing 0.5 M Na^+, respectively.

C.3. QDs deposition on dust.

It was found that QDs deposited on dust particles and remained on working surfaces in the lab. As a result, well-defined fluorescence peaks of QD_{545} and QD_{605} were observed in a background signal from a "clean coverslip". A comprehensive cleaning and improved ventilation were required to bring the background level back to normal.

C.4. References.

(1) Bychkova, V., Shvarev, A. *Anal. Chem.* **2009**, *81*, 7416-7419.

(2) Bakker, E.; Buhlmann, P.; Pretsch, E. *Chem. Rev*. **1997**, *97*, 3083-3132.

APPENDIX D

EXPERIMENTAL DETAILS ON A REPORTING MICROPARTICLE FABRICATION AND CALIBRATION

D.1. Chemicals and materials.

Chemicals purchased from Sigma-Aldrich (ACS quality) were glucose oxidase (GOx, from *Aspergillus niger*, type X-S, E.C. 1.1.3.4), esterase (Est, from porcine liver, E.C. 3.1.1.1), urease (from jack beans, E.C. 3.5.1.5), high-molecular weight poly(vinyl chloride) (PVC; M.W. ca. 200 kDa), *bis*(2-ethylhexyl) sebacate (DOS), *tert*-butyl calix[4]arene tetraethyl ester (sodium ionophore X), sodium *tetrakis*[3,5-*bis*(trifluoromethyl)phenyl borate (NaTFPB), 9-(diethylamino)-5-octadecanoylimino-5H-benzo[a]phenoxazine (chromoionophore I, ETH 5294), tetrahydrofuran (THF), cyclohexanone, ethylene glycol diethyl ether, polyoxyethylene (23) lauryl ether (Brij-35), acetone, 3-(trimethoxysilyl)propyl methacrylate (Silane A174), D-(+)-glucose, ethyl butyrate and urea.. All other chemicals were purchased from VWR (West Chester, PA). All aqueous solutions were prepared with ultrapure water (18.2 MΩ·cm) from Milli-Q water purification system (Millipore).

D.2. Preparation of membrane cocktail.

The optode microparticle components, the polymer (PVC) and the plasticizer (DOS) were dissolved in 1 mL of a 2:1 mixture of cyclohexanone and ethylene glycol diethyl ether. The cocktail contained 40 mmol/kg sodium ionophore X, 20 mmol/kg·ion-exchanger NaTFPB, and 10 mmol/kg chromoionophore I. THF was added to dilute the polymer solution in the ratio of 1:2.

D.3. Optode microparticles immobilization.

Square cover glass strips (22 × 22 mm) were sonicated in 0.1 M NaOH solution for 10 min, rinsed with water and then sonicated in water for 2 min. The glasses

were then rinsed with acetone and kept in an oven at 120 ˚C for 15 min. The cover glass holder was put into a desiccator with Silane A174 and kept under vacuum for 1 h. A small droplet of the optode microparticles emulsion was deposited on the "wet" cover glass and allowed to dry completely. The cover glasses were conditioned in a 0.1 M TRIS solution at pH 7.5 for 24 hours.

D.4. Optode calibration.

For calibrating the optode microparticle, aqueous solutions containing 0.1 M Na_2SO_4 and a universal buffer (3.3 mM citric acid, 5.5 mM boric acid and 5.0 mM phosphoric acid) were titrated to various pH values with 1 M KOH solution. All experiments were conducted at ambient temperature (23±2 °C). Activity coefficients were calculated according to Debye-Hückel formalism. [2]

Table D.1. The pH values: before and after different input combinations.[a]

Input combination	**0**,**0**	**0**,**1**	**1**,**0**	**1**,**1**
Microparticle size, μm	6.0	7.0	7.0	6.5
Initial pH	6.51	6.39	6.27	6.33
Final pH	6.44	5.17	4.00	4.30
ΔpH	0.07	1.22	2.27	2.03

[a] Note that the pH values generated in situ by the enzyme system were measured by individual optode microparticles.

D.5. References.

(1) Bychkova, V.; Shvarev, A. *Anal. Chem.* **2009**, *81*, 2325-2331.

(2) Meier, P. C. *Anal. Chim. Acta* **1982**, *136*, 363.

APPENDIX E

PHOTORESPONSIVE ION-SELECTIVE OPTICAL SENSORS: EQUILIBRIUM AND NON-EQUILIBRIUM RESPONSE

E.1. Photoresponsive optode composition.

The sensors were fabricated as polymeric spherical particles (details on particles fabrication are provided in Appendix A). The membrane contained 40 mmol/kg sodium ionophore (*tert*-butyl calix[4]arene tetraacetic acid tetraethyl ester), 20 mmol/kg ion-exchanger (sodium tetrakis(4-chlorophenyl)borate, and 10 mmol/kg chromoionophore I (ETH 5294), 45 mmol/kg (2,4-bis(trichloromethyl)-6-(4-methoxystyryl)-1,3,5-triazine) (nonionic PAG), 33% of high molecular weight poly(vinyl chloride) and 66% of bis(2-ethylhexyl) sebacate.

Upon UV illumination PAG produces a strong acid according to the mechanism shown in Figure E.1.

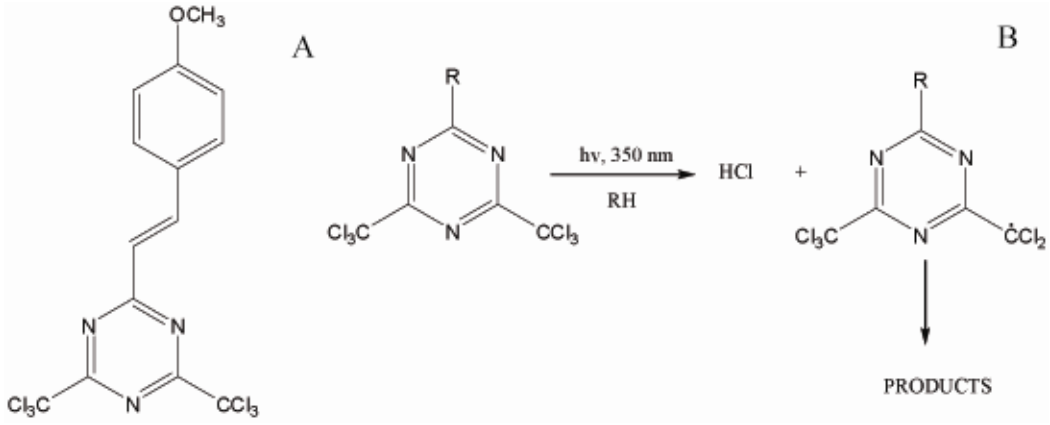

Figure E.1. The structure of 2-(4-methoxystyryl)-4,6-bis(trichloromethyl)-1,3,5-triazine (A) and its photolysis (B).

E.2. Equilibrium and non-equilibrium response.

The optode's equilibrium response was not affected by introduction of an extra component into sensor's matrix. Sodium-selective optodes (with and without PAG) demonstrated the same response function (Figure E.2) and similar ion-exchange constants (log K_{exch} = -5.40 ± 0.05).

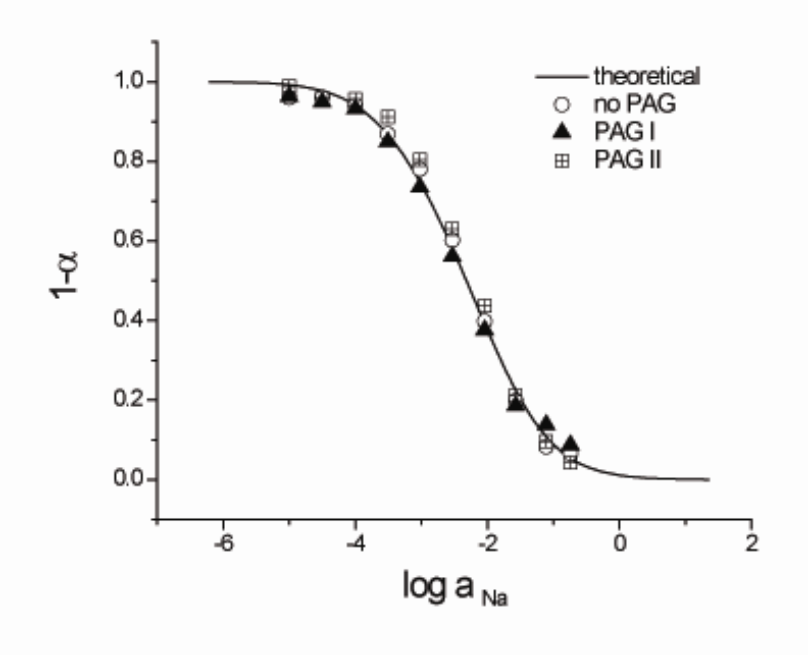

Figure E.2. Calibration curves for the sodium-selective optode with different PAGs and without PAG. The line represents the calculated theoretical[1] response.

When a photoresponsive optode is exposed to UV-light, the protonation degree of the optode increases because of HCl production in the polymer phase. Then hydrogen-ions diffuse into aqueous media, and the optode returns to its initial state. A relaxation process is observed. The resulting relaxation process was fit with an exponential decay function. A good agreement between theoretical[1] and experimental response was obtained (Figure E.3).

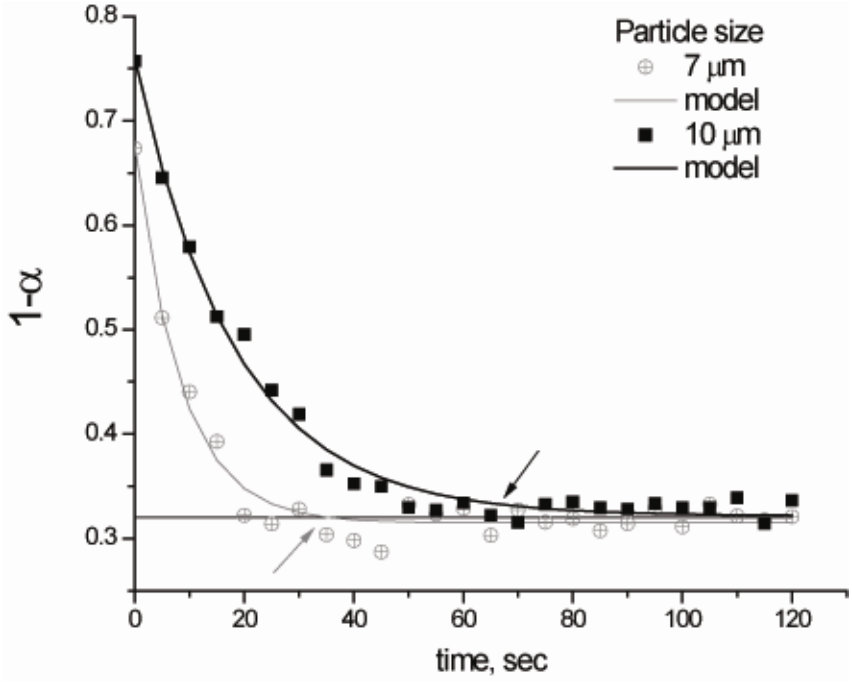

Figure E.3. Non-equilibrium response recorded after 1-s UV exposure. The solution contained 0.001 M NaCl at pH 7.5.

E.3. Simulation of the photoresponsive optode response.

Two approaches were developed to simulate an "active" optode response. A numerical solution was obtained based of finite element analysis using COMSOL Multiphysics software. An analytical solution was obtained independently and confirmed that the relaxation process is indeed an exponential decay:

$$\log\left(\frac{N_t}{N_\infty}\right) = -\frac{\pi^2 D}{ln(10) r_0^2} t + \log\left(\frac{6}{\pi^2}\right) \quad \text{(E.1)}$$

Moreover, compared to the equation of the first order decay:

$$N_t - N_\infty = (N_0 - N_\infty) \cdot \exp(-kt) \quad \text{(E.2)}$$

it allows a relationship between rate constant, *k*, diffusion coefficient in the optode phase, D, and sensing particle radius, r, to obtained:

$$k = \frac{\pi^2 D}{\ln(10) r_0^2} \tag{E.3}$$

The agreement between numerical and analytical solution is excellent for relaxation time values more than 200 ms (Figure E.4).

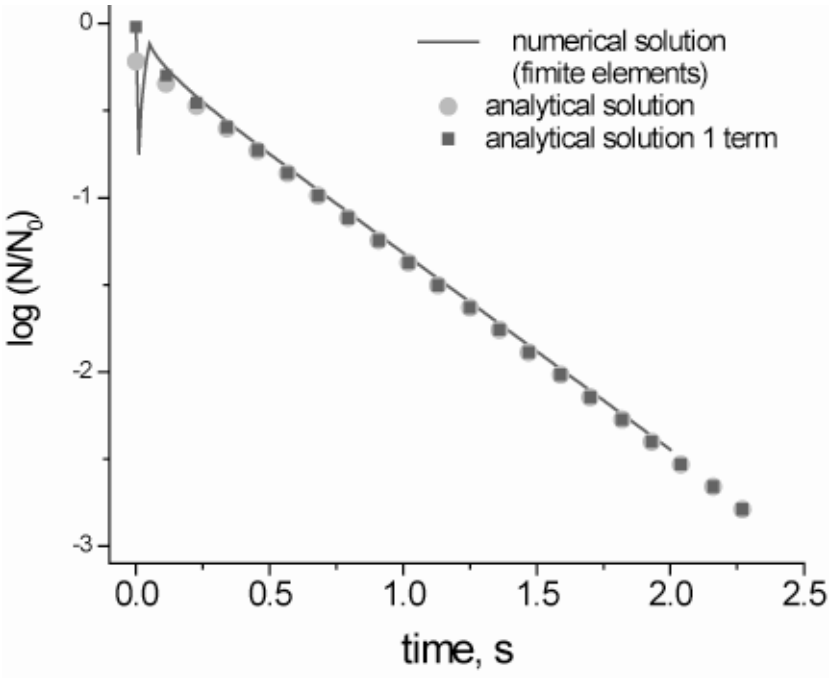

Figure E.4. Agreement between numerical and analytical solution for photoresponsive optode response simulation.

Relaxation of particles of two sizes (7 and 10 μm) in two different buffer concentration (0.001 M and 0.01 M *TRIS*) was monitored. Three batches made on different days and three ages of fabricated emulsion were also compared. Based on a model with a spherical diffusion obeying an exponential decay the rate constant was calculated. Unfortunately, no statistically significant correlation between rate constant and any of the varied parameters was observed. However,

it was possible to estimate a diffusion coefficient in polymeric matrix based on the average rate constant of all experiments – k = 0.079 s^{-1} – and eq.E.3. It was found to be $0.5 \cdot 10^{-12}$ m^2/s which is within an order of magnitude with a literature value – $1.0 \cdot 10^{-12}$ m^2/s.[2] This excellent correspondence confirms that the analytical solution is correct overall, and can be used to describe a relaxation of an "active" optode. However, a numerical solution could be improved by considering chemical reactions in polymeric and aqueous phases, and at the interface.

E.4. References.

(1) Bakker, E.; Buhlmann, P.; Pretsch, E. *Chem. Rev*. **1997**, *97*, 3083-3132.

(2) Schneider, B.; Zwickl, T.; Federer, B.; Pretsch, E.; Lindner, E. *Anal. Chem.* **1996**, *68*, 4342-4350.